Evaluation of the efficiency of magnets in deflecting Ag-atoms in the PBMR-Magnetic Isotope Scrubber (MIS)

by

Joyce Keneilwe Mokgantshang

A mini-dissertation submitted to the faculty of Agriculture, science and technology in partial fulfillment of the requirements for a Master of Science degree in Applied Radiation Science and Technology, North-West University.

Supervisor: Mr. R.T Dobson

Co-Supervisor: Prof G.C Hillhouse

Department of Mechanical Engineering

University of Stellenbosch
and

North-West University

Declaration

I, the undersigned, Joyce Keneilwe Mokgantshang, hereby declare that the work presented in this dissertation except where otherwise indicated, is my own original work and has not been submitted to any university for the purpose of obtaining a degree.

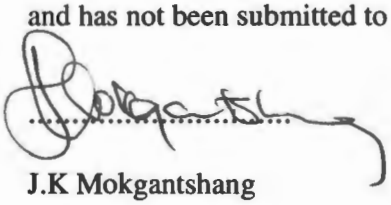

.....

J.K Mokgantshang

.....

May 2008

Abstract

The South-African Pebble Bed Modular Reactor (PBMR) is a high temperature gas cooled reactor (HTGCR) which uses the inert gas helium as a coolant and coated particles as fuel. The design of these coated particles is such that they are able to form a protective barrier against the release of radioactive fission products up to a temperature of 1600 °C under the reactor operating conditions (Ogawa T., et al. 1985). It has been observed from the already proven fuel that the coating layers of these coated particles are not effective against the release of silver (Heather J.M., Ronald G.B., 2004). Of great concern is the release of Ag-110m which has a half-life of 253 days and is an $\beta - \gamma$ emitter when decaying to its Cd stable state (Leena Joseph, et al., 2007).

The released silver is therefore able to enter into the helium gas which is circulating through the reactor power conversion circuit and upon reaching the cooler sides, silver will start to plate out. This constitutes a maintenance problem as ten half-lives have to elapse before normal maintenance can be done. This also poses a radiation hazard to operating personnel and to the members of the public in case of accidental leakage of helium into the environment.

This has led to the proposal of the installation of the Magnetic Isotope Scrubber (MIS) into the hot-pipe section of the reactor in order to remove silver from helium before entering into the Power Conversion Unit (PCU). The scrubber will consist of two components: magnets, either permanent or electro-magnetic, to produce the magnetic field needed to deflect silver atoms, and an atom catcher to catch and contain the radioactive silver atoms. The technique is based on the Stern-Gerlach principle.

The focus of this study was therefore to determine the efficiency of magnets in deflecting silver atoms to a specified position. This was achieved by designing and manufacturing a Magnetic Scrubber Model (MSM), and using it to study the efficiency of magnets. In the experiment a beam of silver atoms was created in an oven by evaporating 99.99 % pure

silver pellets at a temperature of ± 600 °C under a vacuum pressure of 1 x10 $^{-5}$ Torr. The beam was collimated to 2 mm and was allowed to enter the flight tube surrounded by magnets thereby hitting the target which was placed at a specified position. The magnets used were permanent rare earth magnets know as NIB (Neodymium, Iron, Boron) and were orientated to produce a magnetic field intensity of 0.5 Tesla (T) in the centre of the flight tube. The deflection of silver was carried out at different target positions, 12.5, 25.0, 37.5, 50.0 and 75.0 mm with reference to the oven exit and corresponding magnet lengths were used.

The obtained results showed that at shorter distances and shorter magnet lengths the Ag-atoms are less or not at all deflected whereas at longer target position and longer magnets they are strongly deflected. It is therefore concluded that it is important to carry out the deflection over a long range to allow for greater deflection of Ag-atoms.

Dedication

This work is a special dedication to my late mother

Esther Morwenyane Mokgantshang.

Acknowledgements

In this work, I would firstly like to thank the **Almighty God** for the grace and mercy bestowed on me throughout the years of my studies.

My sincere gratitude to the **Centre of Applied Radiation Science and Technology (CARST),** North-west University for presenting me with this study opportunity.

PBMR (Pty) Ltd for the generous financial support, **Stellenbosch University** for the research opportunity and in particular;

My supervisors, **Prof G.C Hillhouse** and **Mr. R.T Dobson** for their immeasurable support and guidance for without them I wouldn't have made it.

The **Department of Physics** group for their valuable contribution to this work.

The **Department of Mechanical Engineering, Sentraal Meganiese Dienste** (SMD) especially **Jackie Bloem,** for the design drawings and **Jos Weerdenburg,** for the manufacture.

Ulrich Buttner, for his knowledge, patience, support and the great contribution he made to this work.

Ockert Kritzinger and **Jacobus Zietsmann** for the technical assistance.

Finally I would like to thank **Mokgantshang** family, for the unfailing love and immeasurable support they gave me during my years of studies.

My sincere gratitude to my Dad. **Douglas Kebonemodisa Mokgantshang**, for making it possible for me to achieve this degree as well as friends, colleagues and to everyone who has made an input towards the achievement of this degree.

A phenomenal Thank You to All of You.

Contents

List of Figures

List of Tables

Nomenclature

Abbreviations:

LOCA	Loss of coolant accident
HTGCR	High temperature gas cooled reactor
IPyC	Inner pyrolytic carbon
MIS	Magnetic Isotope Scrubber
MW	Mega watt
MPS	Main power system
PBMR	Pebble Bed Modular Reactor
PCU	Power conversion Unit
PyC	Pyrolytic carbon
RU	Reactor unit
SiC	Silicon carbide

Symbols:

a	acceleration
B	Magnetic field intensity
d_m	Distance traveled in the magnetic field
d_t	Distance traveled after magnetic field before hitting the target
F	Force
g	Gyromagnetic factor
J	Total angular momentum
K_E	Kinetic energy
l	Length
L	Orbital angular momentum

m	mass
m_s	Spin magnetic moment
S	Total spin of an electron
t	time
v	velocity

Subscripts:

e	electron
g	gap
m	magnet
s	spin
t	target
z	z-direction in the xyz plane

Greek symbols:

α	Probable velocity of atom coming out of the oven
β	Beta particle
γ	Gamma ray
μ_B	Bohr magneton
μ_s	Intrinsic spin magnetic moment
μ_z	Magnitude of spin magnetic moment

1. Introduction

1.1. General overview of PBMR

The South-African Pebble Bed Modular Reactor (PBMR) is a High Temperature Gas Cooled Reactor (HTGCR) which uses an inert gas, helium as a coolant and coated particles as fuel. A single PBMR unit can produce about 165 MW of electricity as a standalone unit or as part of a power plant which may consists of up to six (6) units and it is an inherently safe nuclear reactor (George A.P., 2001). The unit is made up of a Main Power System (MPS) which is divided into two major components directly coupled together, the reactor unit (RU) and the Power Conversion Unit (PCU) as shown in Figure 1.

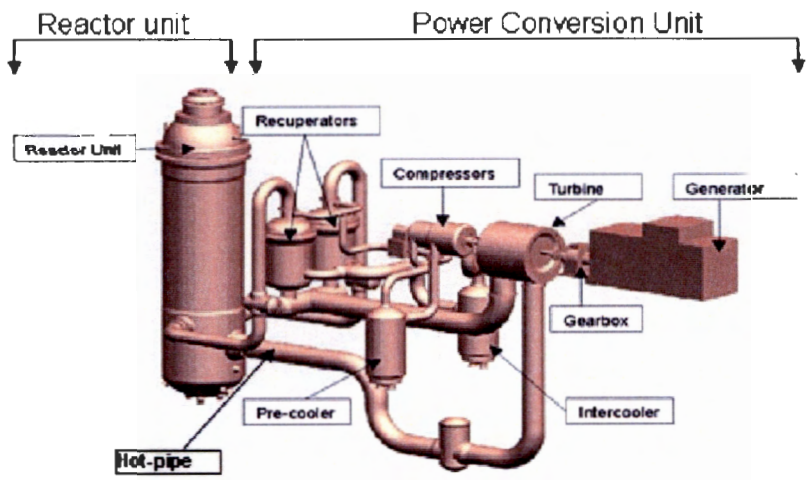

Figure 1. The PBMR-Main Power System (Martzer 2004).

Figure 1 is a schematic layout of the PBMR-MPS showing the two major components and their respective sub-components. This study is only limited to the hot-pipe section of the reactor.

In the PBMR, the electricity production is a two stage process, the transfer of heat energy generated from fission chain reaction in the reactor core to the helium gas in the RU and the conversion of heat energy from helium into electricity in the PCU.

1.1.1. The reactor unit

The reactor unit is a thick walled vertical steel pressure vessel which is approximately 27 m high and 6.2 m in diameter and it houses the reactor core (refer to Figure 2). The design of the tall and slender core geometry helps to limit the maximum temperature reached during loss of coolant accident conditions (LOCA) up to 1600 °C. The core is loaded with approximately 452 000 fuel spheres and this is where fission chain-reactions of U-235 take place (George A.P., 2001). During fission a variety of fission products can be formed and in the process a lot of energy in the form of heat is released.

1.1.2. Power Conversion unit (PCU)

The power conversion unit is where the conversion of heat energy into electrical energy takes place. Helium enters the PCU through the hot-outlet pipe and flows to the Power turbine, recuperator, pre-cooler, low pressure compressor, inter-cooler, high pressure compressor, recuperator and then flows back to the reactor core thus forming a closed coolant cycle (refer to Figure 2 below).

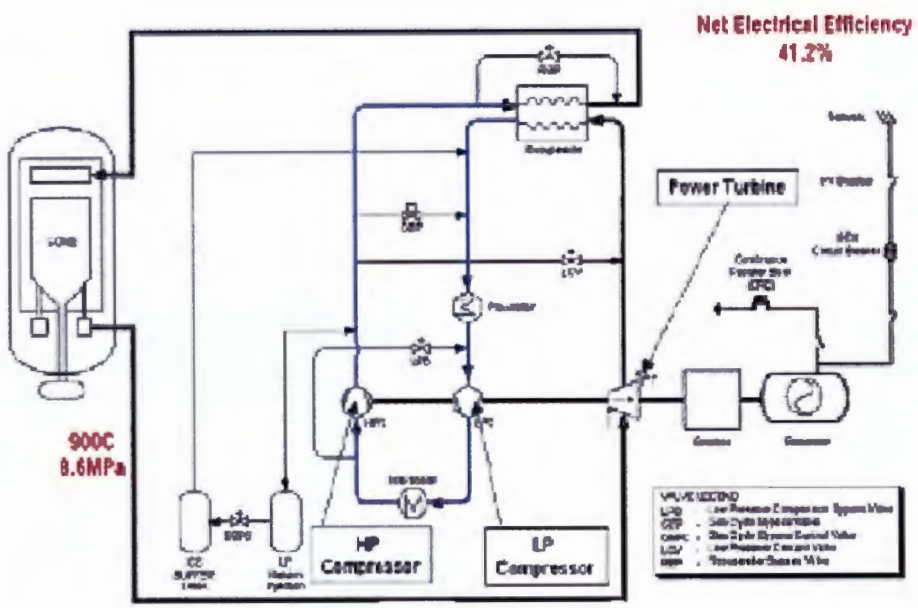

Figure 2. Schematic layout of PBMR-MPS (Slabber J., iThemba LABS presentation 2004).

Figure 2 is a schematic layout of the PBMR-MPS, in the picture the arrows indicate the direction of helium flow in the reactor circuit.

1.1.2.1. Simple ideal Brayton cycle

The Simple Brayton cycle is a thermodynamic process in which heat exchange is taking place in the PBMR. It requires no intermediate heat exchanger between the primary and the secondary cycle. The cycle consists of two isentropic and two isobaric processes as shown in Figure 3.

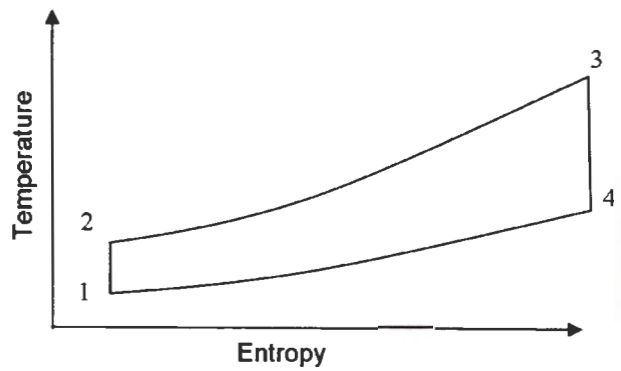

Figure 3. The simple ideal Brayton cycle (George A.P., 2001).

In Figure 3; at point 1, helium gas at low temperature and pressure is compressed in an isentropic process to a higher pressure and temperature to point 2. From points 2 - 3 the gas is heated in an isobaric (constant pressure) process to the maximum cycle temperature. From points 3 - 4 the hot-high pressure gas is expanded isentropically in a turbine to a lower pressure and temperature and the cycle is completed from points 4 - 1 by cooling the gas at constant pressure (George, A.P., 2001).

1.1.3. The fuel spheres

The fuel used for the PBMR consists of 60 mm diameter fuel spheres based on a German design and each sphere contains about 14 500 coated particles embedded in a graphite matrix and surrounded by 5 mm graphite layer as shown Figure 4 (George A.P., 2001., Nabielik H., et al., 1985).

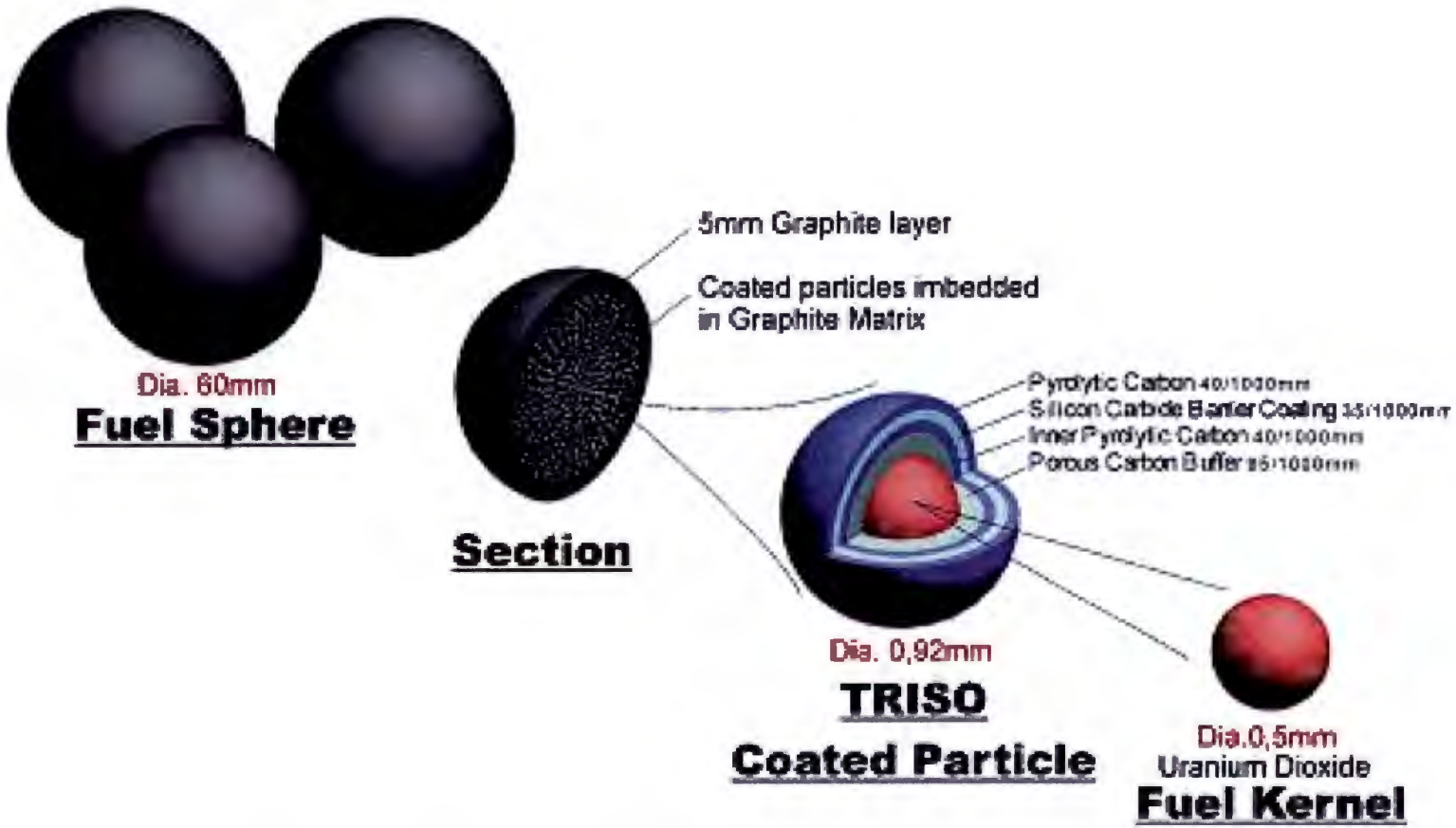

Figure 4. The cross-sectional view of coated particles (Slabber J., iThemba LABS presentation 2004).

Each coated particle consists of a 0.5 mm fuel kernel which is made up of about 10% enriched UO_2 and is covered with four layers, the porous carbon buffer layer, inner pyrolytic carbon layer (IPyC), Silicon carbide layer (SiC) and the Pyrolytic carbon (PyC) layer as shown in Figure 4.

The design of these coated particles limits the release of fission products into the coolant except for silver. Silver is the only known element released out of the coated particles into the coolant at any temperature above 1150 °C when the reactor starts to heats up (Nabielek H., et al., 1985). The release occurs on intact coated particles, failed particles and also from as-manufacture defective particles (Inamati S.B., et al., van der Merwe J.J., 2004). The amount of released silver is initially small and occurs as the pebble heats up and this is strongly dependent on the temperature of the core (Slabber J., 2004).

1.1.4. Heat transfer process

During nuclear fission-chain reactions in the reactor core a lot of energy in the form of heat is generated and needs to be carried away from the reactor core to the PCU for conversion into electricity. The heat transfer process is facilitated by the helium gas which flows continuously through the reactor circuit.

Helium enters the top of the reactor core, being heated to a temperature of 500 °C and a pressure of 8.4 MPa. It then flows vertically downwards in between the fuel spheres and leaves the bottom being heated to a temperature of 900 °C silver will thus be carried away during the process and upon reaching the cooler sides it will start to plate out.

This results in increased radioactivity levels in the MPS and this poses a radiation hazard to operating personnel when scheduled maintenance has to be done and also to the members of the public in case of loss of coolant accident conditions (LOCA), since helium is a gas that leaks easily even from airtight valves. This has subsequently led to the proposal of the installation of a MIS in the hot-outlet pipe section of the reactor as a means of removing silver from helium before entering the PCU.

1.1.5. Magnetic Isotope Scrubber (MIS)

The proposed MIS for PBMR will be placed in the hot-outlet pipe of the PBMR and will be used to catch and remove Ag-atoms from the hot-helium outlet pipe by deflecting them to a pipe wall before they enter the PCU through the use of magnets. The structure will consist of magnets which could either be permanent or electro-magnets aligned along the length of the hot-pipe and an atom catcher inside the hot pipe as shown in Figure 5.

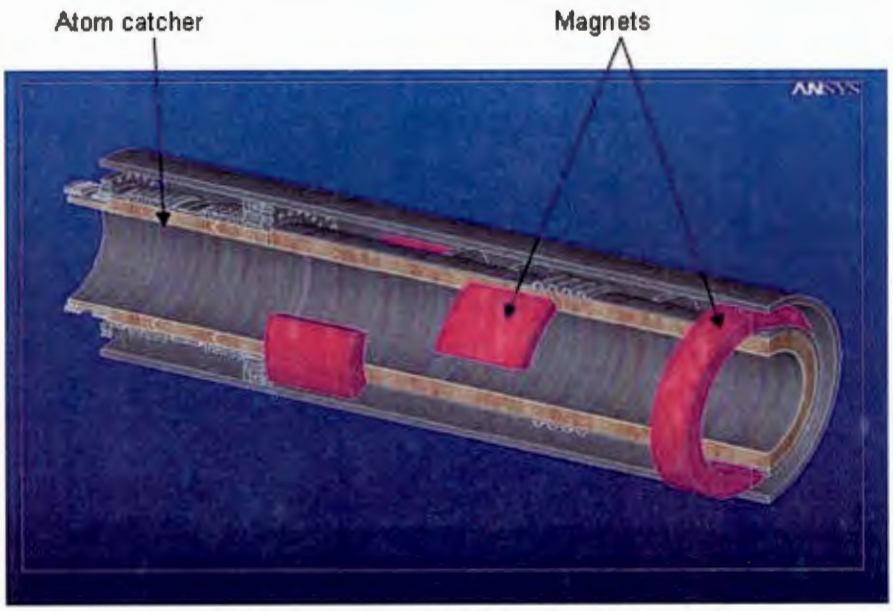

Figure 5. The proposed MIS (Kuczynski L., 2001).

These magnets are used to produce the magnetic field needed to deflect Ag-atoms to the atom catcher based on the Stern-Gerlach principle. The atom catcher is a multilayered deposition ring lined inside the hot-pipe and will be used to catch and contain all the radioactive Ag-atoms from helium before entering the PCU. This structure can be removed at the end of the PBMR life-cycle and sent for long term storage.

1.1.6. The advantages of using helium as a coolant

The choice of using helium as a coolant gas is mainly attributed to the following characteristics:

i. It is chemically inert and will not become radioactive while coming in contact with neutrons; only a small amount of He-3 will be activated

ii. It has a high thermal capacity and good heat transfer inside the reactor can be achieved

iii. It can be used at high temperatures and hence and therefore a high cycle thermal efficiency can be achieved and hence efficiency electricity production

iv. In addition, a high temperature allows the use of heat for other technological purposes and amongst others is the production of hydrogen from water (Ponomarev-Stepnooi et al., 2003).

1.1.7 Problem statement

Ag-110m is a long lived metallic fission product formed inside the nuclear reactor core which is released out of the coated particles at any temperature above 1150 °C when the reactor starts to heat up during operation. It is therefore able to reach the surface of the reactor core and enter the helium coolant which is flowing throughout the reactor. The Ag-110m will thus be circulated through the reactor circuit until it reaches the cooler sides of the MPS where it will start to plate out. Ag-110m has a relatively long half-life of 253 days and has two possible modes of decay to the Cd-110 ground state and this is accompanied by β and γ-ray emissions. This results in the contamination of the coolant and of the MPS which results in a radiation hazard to members of the public in case of loss of coolant accident conditions (LOCA) and to operating personnel when scheduled maintenance has to be done to the reactor.

1.1.8 Objectives

1. To build a Magnetic Scrubber and this will be used to evaluate the efficiency of magnets in deflecting Ag-atoms to a specified target plate using a modified Stern-Gerlach principle. This experiment will be carried out under vacuum conditions as opposed to the PBMR-working conditions.

2. To study the efficiency of the PBMR magnetic isotope scrubber in removing Ag-atoms from the hot-helium outlet pipe by deflecting and catching them on a specified target before entering the PCU.

1.1.9. Motivation

The motivation for this study is to minimize radioactive contamination of the primary circuit in order to facilitate inspection and maintenance and the protection of the personnel and the public.

2. Literature survey

2.1. The formation of Ag-110m

Ag-110m is a long-lived metallic fission product formed inside the nuclear reactor as a result of fission chain reactions of U-235 which is a fissile material in the nuclear reactor. When U-235 comes into contact with one of the neutrons inside the nuclear reactor, the U-235 will capture a neutron to form an excited U-236 nucleus and there are two possible reactions that can occur from this excited nucleus. It could either undergo fission or rid itself off its excess energy by emitting a gamma ray to form a stable U-236 and in this case it will be no longer of interest as far as fission is concerned (Gregg King C.D., 2nd Edition). The reaction is shown by the nuclear equation below

$$ {}_{92}U^{235} + {}_{0}n^{1} \rightarrow {}_{92}U^{236*} \begin{cases} \rightarrow {}_{z_1}F^{A_1} + {}_{z_2}F^{A_2} + 2.5n + energy \\ \rightarrow {}_{92}U^{236} + \gamma \end{cases} \qquad (2.1) $$

During the fission process the two fragments are formed and are denoted by F_1 and F_2 because fission can result in a wide variety of fragments with mass numbers ranging from 70 to 160, an average of 2.5 neutrons and energy are released. It is through the fission process that silver is formed in the nuclear reactor. It is initially formed as a stable isotope which is Ag-109 and following neutron capture it is converted to Ag-110m (Ogawa T., et al., 1985).

$$ {}_{47}Ag^{109} + {}_{0}n^{1} \rightarrow {}_{47}Ag^{110m} + \gamma \qquad (2.2) $$

2.2. The decay of Ag-110m

The formed Ag-110m is in an isomeric state and therefore has two possible modes of decay as shown by the nuclear equation below. It can decay directly to the stable Cd-110 state or via the metastable state to the Cd-110 stable state (Leena J., et al., 2007).

$$_{47}Ag^{110m} \xrightarrow{253(1.14\%)} {}_{47}Ag^{110} + \gamma \xrightarrow{24s} {}_{48}Cd^{110} + \beta^- \tag{2.3}$$

or

$$_{47}Ag^{110m} \xrightarrow{253\,days(98\%)} {}_{48}Cd^{110} + \beta^- \tag{2.4}$$

The formed radio-nuclide is an $\beta - \gamma$ emitter with a complex decay scheme as shown schematically in Figure 6.

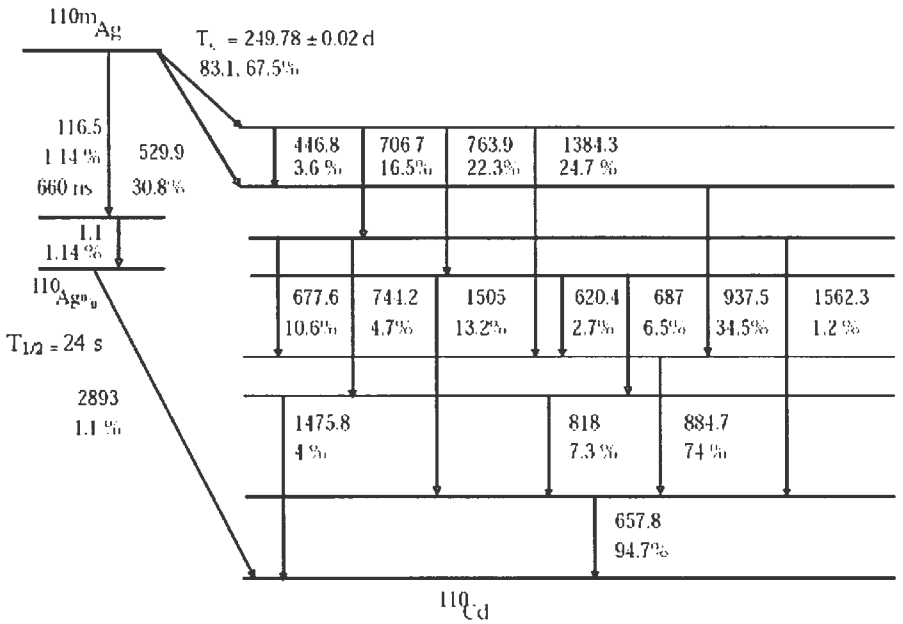

Figure 6. Simplified decay scheme of Ag-110m (All energies are in keV and intensities are absolute) Leena J., 2007).

In Figure 6 the radionuclide Ag-110m has three principal modes of decay, a 116.5 keV γ-transition (1.14 %) to Ag-110 which further decays in 24.5 s by β–emission to the ground state of Cd-110 and the two strong β–transitions (67.5% and 30.8%) with end-point

energies of 83.1 and 529.9 keV respectively which leads to the excited state of the Cd-110 daughter nucleus. The subsequent decay of this excited Cd-110 nucleus consists of more than 50 γ-ray transitions (Funk, E.G., Wiedenbeck M.L., 1958, Scott S.A., Taylor H., 1959).

2.2.1 Gamma rays (γ)

Gamma-rays are a form of electromagnetic radiation which is emitted due transitions between energy levels within the nucleus and can be characterized by the following factors:

i. They have a high energy and high frequency which can cause serious damage when absorbed in tissue.
ii. High penetrating ability in matter and in tissue which makes their attenuation difficult.
iii. They are able to cause secondary interactions when passing through matter and tissue.

The energy of gamma rays can be absorbed by three processes, namely; photoelectric effect, Compton scattering and pair production.

2.2.1.1. Photoelectric effect

The photoelectric effect is a common process for low energy gammas and it gives total energy absorption. In the process an incident gamma-ray knocks out an atomic electron by transferring all its energy to it and it ceases to exist. It is thus absorbed in the process as illustrated schematically in Figure 7. To conserve energy and momentum a photo-electron is then emitted.

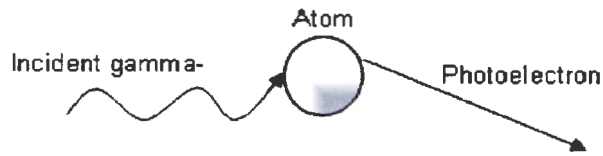

Figure 7. The schematic diagram of the photoelectric process.

2.2.1.2. Compton scattering

The Compton scattering is an elastic process that occurs between the gamma ray and a loosely bound electron, but does not involve the entire atom. In the process an incident gamma-ray of a given energy strikes a loosely bound electron and is scattered in an elastic collision from the original path with a reduced energy as illustrated in Figure 8 and this energy is transferred to the electron. Momentum and kinetic are conserved in the process and it occurs over all energy ranges.

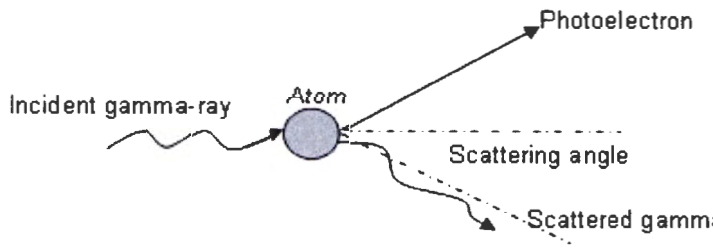

Figure 8. Schematic diagram of a Compton scattering process.

2.2.1.3 Pair production

Pair production is an effective energy absorption process which occurs for high energy gammas with energy in excess of 1.02 MeV under the influence of the Coulomb field of the nucleus to create and an electron-positron pair (refer to Figure 9). The positron is relatively short lived and will combine with an electron. Two 0.51 MeV gamma rays can be formed resulting in the absorption of energy; note however that one or both gamma-rays can escape without depositing energy.

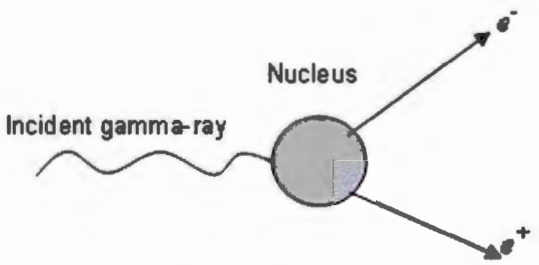

Figure 9. Schematic diagram of a pair production process.

2.2.2 The release of Ag-110m

The release of silver occurs on intact coated particles and there is no complete understanding of the release phenomena available but the role of temperature is regarded as being critical (Petti et al., 2003, Heather, J.M., Ronald, G.B., 2004). There is however factors which can be considered to influence the release of silver under both normal and abnormal operating temperature conditions and these are listed below:

2.2.2.1. Normal operating conditions

During normal reactor operating conditions the release of silver could be influenced by heavy metal contamination of the graphite matrix and initially defective particles. The contaminated graphite matrix results in fission products being formed outside the coating layers and this makes it possible for them to be freely released into the coolant. The defective particles are the result of as-manufactured defects. It is estimated that a small fraction (about 2/14 500) of coated particles will have defects and during irradiation they will start to fail and release the fission products into the coolant (Heather et al., 2002., Petti et al., 2004).

2.2.2.2. Abnormal operating conditions

Coated particle failure under high irradiation temperature as a result of LOCA which can be caused by either one of the following failure mechanisms, pressure vessel failure, fuel kernel migration, interactions of fission products with the coating layers, SiC thermal decomposition, cracking of pyrocarbon layer, matrix-outer pyrocarbon interaction and SiC degradation (Nabielik, H. et al., 1985).

This results in the destruction of the coating layers and makes it possible for Ag-110m to be released freely out of the coated particles into helium coolant. Figure 10 is one example of a coated particle whose layers have been damaged.

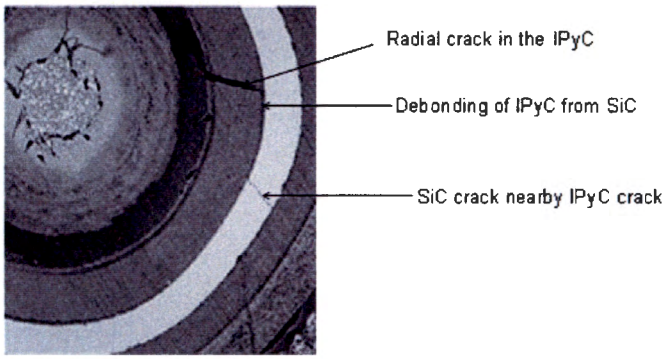

Figure 10. Photo-micrograph of a coated particle showing radiation induced cracks on coating layers (Petti et al., 2003).

In Figure 10 a radial crack appears in the IPyC and SiC layer, the IPyC is de-bonding from the SiC and therefore it is possible for Ag-110m to diffuse out freely through this radial cracks into the coolant. It will remain in the coolant until it decays to the Cd-110 stable state.

3. Applicable theory

3.1 Stern-Gerlach principle

The operation of the Magnetic isotope scrubber is based on the Stern-Gerlach principle whereby Ag atoms are deflected through the use of magnets. The experiment was first performed in 1921 by Otto Stern and Walter Gerlach and they were able to demonstrate the quantization of spin into two orientations (Liebermann J., 1998). The actual experiment was carried out with a beam of silver atoms because they could be easily detected using photographic emulsion. In the experiment a beam of Ag-atoms was generated by evaporating liquid metal silver from a hot oven and the atom beam was collimated by slits and sent through a region with a large non-uniform magnetic field as shown schematically in Figure 11.

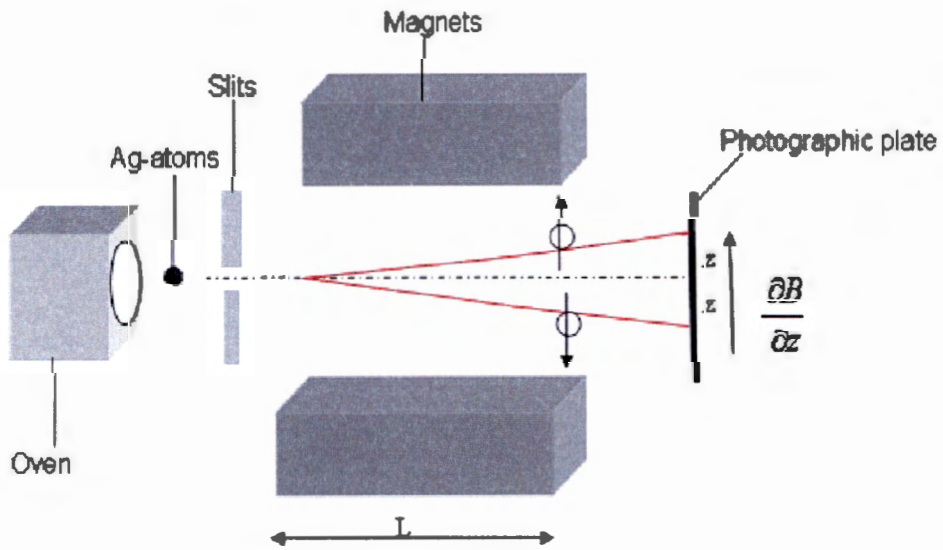

Figure 11. The Stern-Gerlach experimental set-up.

The purpose of the non-uniform magnetic field is to produce a deflecting force on any magnetic moments that are present in the field (Gauntreau, R., and Savin, W., 2nd Edition). The process was performed in vacuum so that silver atoms move without scattering. In the experiment it was found that when the beam strikes the photographic

plate it has split into two distinct parts, with equal number of atoms distributed above and below the point when there is no magnetic field.

3.1.1. Electronic configuration of Ag

The ground state electron configuration for Ag-109 is $[Kr]4d^{10}5s^1$, and is schematically shown in Figure 12 below

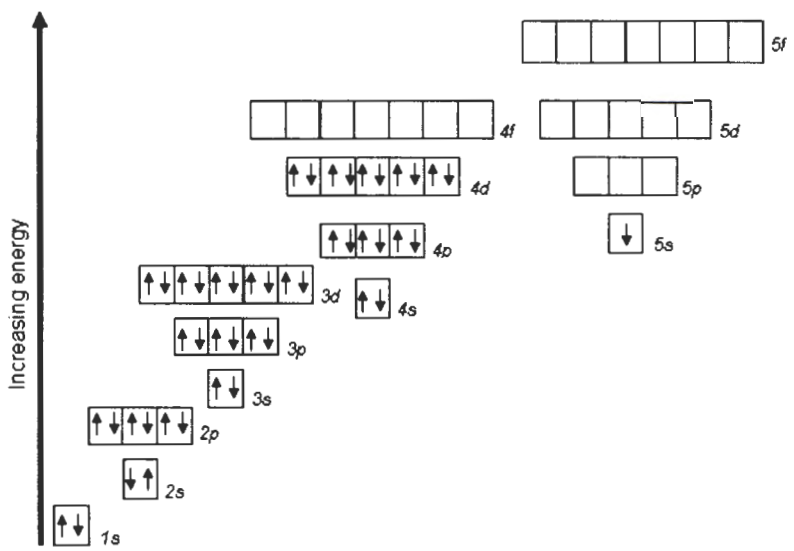

Figure 12. The ground-state electron configuration of Ag-109.

In Figure 12 all electrons in the shells are paired except for the $5s^1$ shell with one unpaired electron, all paired electrons couple to zero spin magnetic moment. This unpaired electron therefore possesses a spin magnetic moment which causes the atom to interact with the external magnetic field.

3.1.2 Electron spin and angular momentum

From quantum mechanics we know that the total angular momentum is given by the expression,

$$\vec{J} = \vec{L} + \vec{S} \tag{3.1}$$

where J total angular momentum

L orbital angular momentum

S total spin of an electron

The electron spin is quantized and assumes an integer value, ($S_z = \pm 1/2\hbar$); it is an intrinsic property of an electron; it determines the electron's magnetic dipole moment in a magnetic field and is independent of other quantum numbers J and L (http://hyperphysics.phy-astr.gsu.edu/hbase/spin.html).

3.1.3 The electron spin magnetic moment

The Ag-atom outer electron has an intrinsic angular momentum and it was expected to be similar to the magnetic moment of an electron orbit. Therefore the z-component of the magnetic moment associated with the electron spin was expected to be (http://hyperphysics, phy-astr.gsu.edu/hbase/spin.html)

$$\mu_e = \pm\frac{1}{2}\mu_B . \tag{3.2}$$

But the measured value for the electron spin is written as

$$\mu_S = \pm\frac{1}{2} g\mu_B \tag{3.3}$$

where g Gyromagnetic factor

μ_B Bohr magneton, a natural constant which arises in the treatment of magnetic fields.

Therefore

$$\mu_s = \mu_B . \tag{3.3}$$

3.1.4. Calculation of magnetic deflection

The deflecting force acting on the Ag-atoms for the situation in Figure 11 is directly proportional to the magnetic field gradient and is given by the following expression

$$F_z = \mu_s \cos\theta \frac{\partial B}{\partial z} \tag{3.5}$$

where θ is the angle between μ_s and μ_B, and $\partial B/\partial z$ is the gradient of the non-uniform field but along the beam axis, $\partial B_x/\partial x = 0$ (by symmetry) and $\partial B_x/\partial x$ (by antisymmetry); also $\partial B_x/\partial x$ will be very small. Consequently $F_x \approx 0$, $F_y = 0$ and F_z = maximum force experienced by the silver atoms.

The electron spin magnetic moment has a potential energy (U), in a magnetic field (B) applied in the z-direction and is expressed as

$$U = \mu_z B_z = \mu_B \frac{g}{2} B_z = \pm \mu_B B_z. \tag{3.6}$$

Using the relationship of force to potential energy gives

$$F_z = \frac{\partial U}{\partial z} = \pm \mu_B \frac{\partial B_Z}{\partial z}. \tag{3.7}$$

For this experiment the magnetic circuit must be designed such that there is a region of constant ($\partial B_z/\partial x$ = constant $\Rightarrow$ F_Z = constant) NB: this is the gradient of the magnetic field then the beam will split into two distinct beams.

3.1.4.1 The distance of deflection (z)

In the Stern-Gerlach experimental set-up a beam of Ag-atoms is directed along the y-axis and splits slightly along the z-axis (refer to Figure 13). It is therefore possible to calculate the deflection of Ag-atoms (z) with a mass m, and velocity v, by assuming that the deflection force is constant in the region of the beam and zero everywhere else.

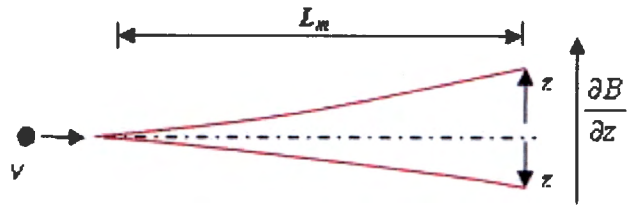

Figure 13. Illustration of a deflection principle (Liebermann J., 1998).

Then from Newton's second law of motion the distance of deflection (also called z-deflection) z-expression is defined as

$$z = \frac{1}{2}at^2 = \frac{1}{2}\frac{F}{m}\left(\frac{L_m}{v}\right)^2 = \pm\frac{\mu_{B_z} L_m^{\,2}}{4K_E}\frac{\partial B_z}{\partial z} \qquad (3.8)$$

where

z	deflection of Ag-atoms
a	acceleration of Ag-atoms
t	time taken in the magnetic field
F_z	deflecting force in the z-direction
m_{Ag}	mass of Ag atoms
L_m	distance traveled in the magnetic field
v	velocity of Ag-atoms
μ_B	constant (Bohr magneton)
K_E	kinetic energy of Ag-atoms
$\frac{\partial B_z}{\partial z}$	Magnetic field gradient.

3.1.4.2. The distance of deflection (z) on the target plate

In order to calculate the distance of deflection, z when we have a target placed at a specified position the distance traveled by the Ag-atoms after exiting the magnetic field region to the target plate must be considered as shown schematically in Figure 14.

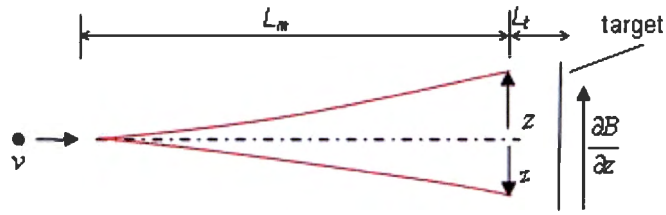

Figure 14. Illustration of a deflection principle on a target (Liebermann J., 1998).

In Figure 14 the Ag-atoms travel in the region of the non-uniform magnetic for a distance L_m, after exiting it travels a distance L_t before reaching the target plate. Therefore the total z will now be

$$z = \frac{1}{2} a t_1^{\,2} + v t_2 \tag{3.9}$$

Where t_1 is the time spent in the non- uniform magnetic field , t_2 is the time spent after exiting the magnetic field but before the target, and where $t_1 = L_m / v$ and $t_2 = L_t / v$

Therefore z will now be

$$z = \pm \frac{1}{2} \frac{F_z}{m_{Ag}} \left(\frac{L_m}{v}\right)^2 + \frac{F_z}{m_{Ag}} \left(\frac{L_m}{v}\right)\left(\frac{L_t}{v}\right) \tag{3.10}$$

Where F_Z is the deflecting force in the z-direction, m_{Ag} is the mass of Ag-atoms, L_m distance traveled in the magnetic field, L_t distance traveled after the magnetic field before hitting the target and v velocity of Ag-atoms.

Following re-arrangement we therefore have

$$z = \frac{F_Z}{m_{Ag} v^2} L_m \left(\frac{L_m}{2} + L_t\right). \tag{3.11}$$

3.1.5. Velocity distribution of Ag-atoms

The Stern-Gerlach experiment is limited to a certain extent by the fact that Ag-atoms emerging from the oven at absolute temperature, T do not have a unique velocity (Liebermann, J., 1998). This velocity distribution of the Ag-atom in the beam is given by

$$I_o(v_o)dv = 2I_o(v/\alpha)^3 e^{-(v/\alpha)^2} d(v/\alpha) \qquad (3.12)$$

This velocity distribution will give rise to the various patterns in deflection of Ag-atoms. Where I_o is the total beam intensity, α most probable velocity of Ag-atom in the oven $\alpha = \sqrt{2kT/M}$, k is the Boltzmann constant, T is the temperature of atoms in Kelvin, and m is the mass of Ag-atoms in Kg

Given $k = 1.38\times10^{-23}\,J.K^{-}$

T = 600 +273 = 873 K (temperature of the oven in the experiment)

M = 1.79×10^{-25} Kg

$\alpha = \sqrt{2 \times 1.38 \times 10^{-23} J.K^{-1}/1.79 \times 10^{-25} kg}$

= 366.88 *m/s.*

This is the probable velocity of the Ag-atoms when they come from the oven at $\pm 600\,^{\circ}C$ in this experiment.

4. Experiment

4.1 Design, manufacture and experimental set-up

A special apparatus has been built in order to demonstrate the efficiency of magnets in removing Ag-atoms by deflecting them to a specified target plate based on Stern-Gerlach principle. The Ag-atom beam was created in an oven by vaporizing pure 99.99% Ag pellets under vacuum pressure of 1 x10 $^{-5}$ Torr. The atom beam was allowed to pass through a region of non-uniform magnetic field and for the purpose of this experiment the beam was allowed to pass through different magnet lengths. The schematic layout of the set-up is shown in Figure 15.

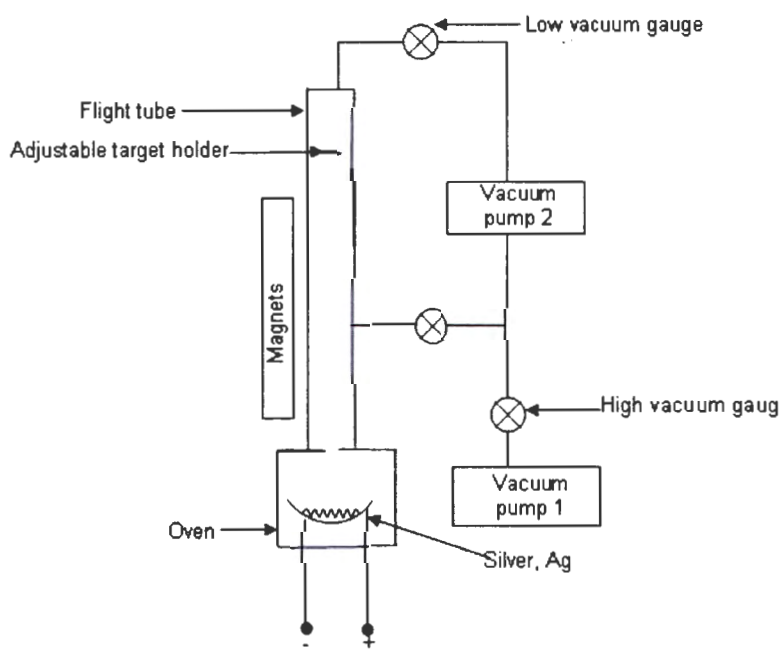

Figure 15. Schematic layout of the experimental set-up.

In Figure 15 the Ag-atom beam is created in the oven by heating Ag-pellets in a crucible and the beam passes into the flight tube which has magnets placed 180 ° around it.

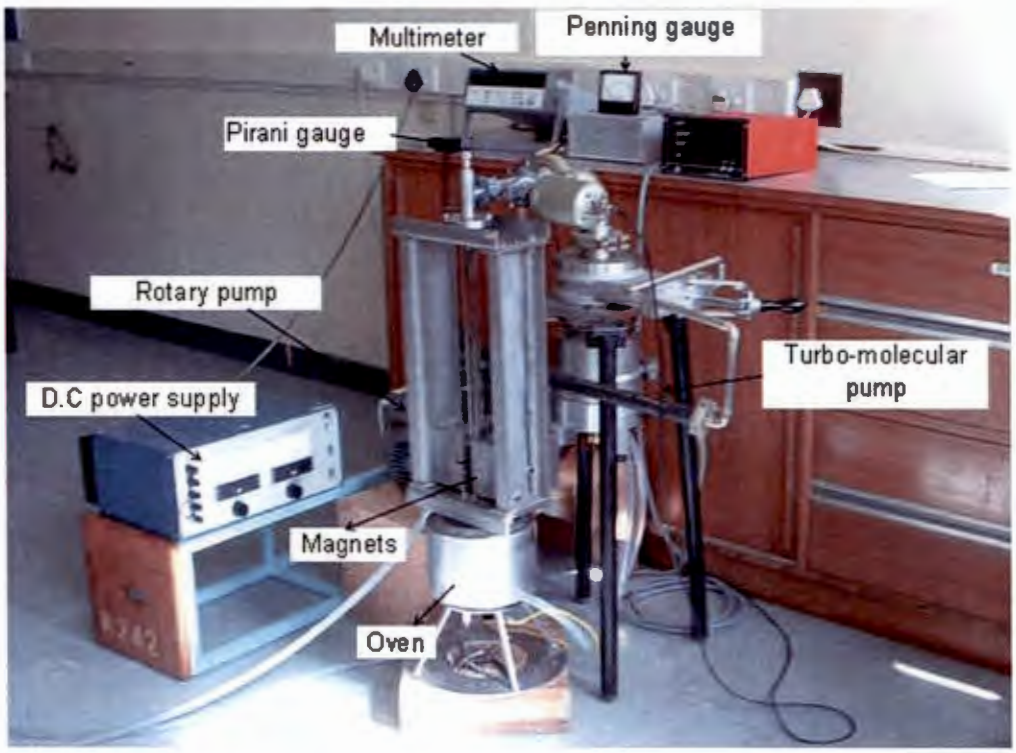

Figure 16. Picture of the experimental set-up.

Within the flight tube there is an adjustable target holder and the targets used are glass slides cut into 16 mm diameter round discs. Also connected to the model are two vacuum pumps namely, a rotary pump (vacuum pump 1) and a turbo-pump (vacuum pump 2). Two vacuum gauges are used for measuring the vacuum pressure within the flight tube, namely a Penning gauge which is used for measuring high vacuum and the Pirani gauge used for low vacuum. The experimental set-up consists of four (4) main parts namely: silver oven, flight tube, the magnetic circuit and the vacuum system and each part is explained below.

4.1.1. The silver oven

The silver oven is made from a non-magnetic stainless steel and is surrounded by a cooling jacket to remove excess heat during the experiment. It is opened from the bottom by removing the bottom flange which consists of two main parts, the crucible and the heating element as shown in Figure 17.

The crucible used is made from porcelain, with a high melting point and is supported on a non-magnetic stainless steel pole. The heating element wire used is a high resistance tungsten wire of resistance ~ 3 Ω with a thickness of 0.225 mm and is wound around the ceramic crucible. It is connected to the external power supply through the anode and the cathode as shown in Figure 17 (b). The oven temperature is monitored through the insertion of a high temperature thermocouple which is connected to a multimeter which is calibrated in °C. The oven temperature was kept at 600 °C just above the melting point of silver and at this temperature a hot Ag-atom beam exits the oven through a 2 mm collimating nozzle into the flight tube.

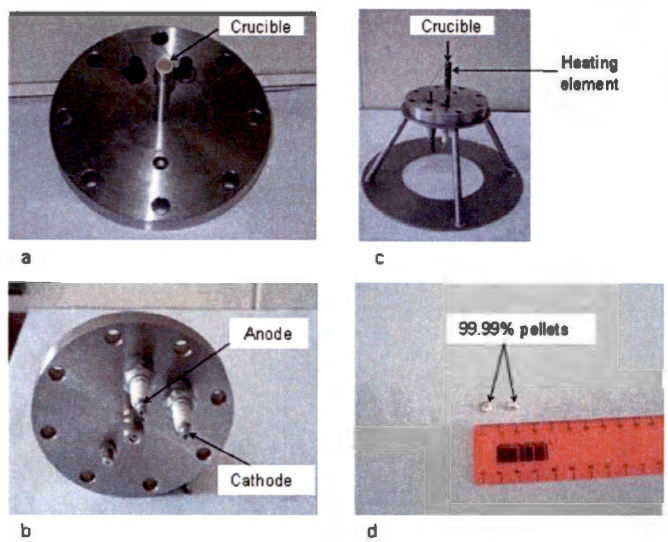

Figure 17. The main parts of the oven.

Figure 17 (a) and (b) shows the top and bottom part of the flange and on the bottom the positive and the negative terminals that lead to the external DC source are shown,(c) stand with the flange (d) Ag pellets used.

4.1.2 The flight tube

The flight tube is a cylindrical glass tube 20 mm in diameter, 28 cm long and consists of an adjustable target holder inside. The targets used are 16 mm diameter round glass slides and they are clamped onto the holder. This tube allows visual monitoring of the oven, the position of the target and the target holder. A vacuum of 1 x 10^{-5} Torr was maintained in the entire region of the flight tube in order to eliminate the collisions between the silver and air atoms.

4.1.3 The magnetic circuit

A C-shaped magnetic circuit was used and the type of magnets used is permanent rare earth magnets which are known as NIB, an acronym for Neodymium Iron Boron. The design approach followed from Ampere's law namely that for a circuit consisting of an air gap, a portion of a permanent magnet and a ferromagnetic portion (Syed, Nasar., 2nd Edition).

$$H_d l_m = H_g l_g + v_{mi} \qquad (4.1)$$

Where H_d magnetic field intensity of the magnet (Oersteds)

l_m length of the magnet (cm)

H_g magnetic field intensity in the gap, (Oersteds) = flux

l_g length of the gap

v_{mi} reluctance drop in the ferromagnetic portion.

Following re-arrangement of the above equation and assuming that the reluctance drop in the soft iron parts of the circuit is negligible, giving a reluctance drop v_{mi} of zero, l_g can be calculated as

$$l_g = \frac{H_d l_m}{H_g} \qquad (4.2)$$

For the design $l_g = l_m = 7.5$ cm

The cross-sectional area of the magnet is calculated from the flux required in the air gap from the relationship

$$B_d \delta_m = K B_g \delta_g \qquad (4.3)$$

where B_d flux density in the magnet, (Gauss)

δ_m cross-sectional area of the magnet, (cm^2)

B_g Cross-sectional area of the gap, (cm^2)

δ_g cross-sectional area of the gap, (cm^2)

K dimensionless leakage factor

Following re-arrangement

$$\delta_m = \frac{K B_g \delta_g}{B_d} \qquad (4.3)$$

Given l_g = 7.5 cm

B_d = 12 000 Gauss (refer to fig A.1)

δ_g $= l_g$ x w_g

= 7.5 cm x 2.8 cm

= $21 cm^2$

The leakage factor, K for the configuration used for the experiment is shown in Figure 18 and it can be determined from the following equation (Syed, A. N., 2nd Edition).

$$K = 1 + \frac{l_g}{\delta_g} 0.67 C_a \left[1.7 \left(\frac{0.67 C_a}{0.67a + l_g} \right) + \frac{l_g}{2a} \right] \qquad (4.4)$$

where C_a cross sectional perimeter of the circuit whose lengths are a, b and c respectively

	0.67	a factor which arises from the fact that permanent magnets have a neutral zone which does not contribute to leakage
Given	a	$2\ cm$
	C_a	$8\ cm$
	l_g	7.5 cm
	δ_g	$21\,\text{cm}^2$

Therefore

$$K = 1 + \frac{7.5\,\text{cm}}{21\,\text{cm}^2} 0.67\,(8\text{cm}) \left[1.7 \left(\frac{0.67(8\,\text{cm})}{0.67(2\,\text{cm}) + 7.5\,\text{cm}} \right) + \frac{7.5\,\text{cm}}{2(2\text{cm})} \right]$$

$$= 6.7$$

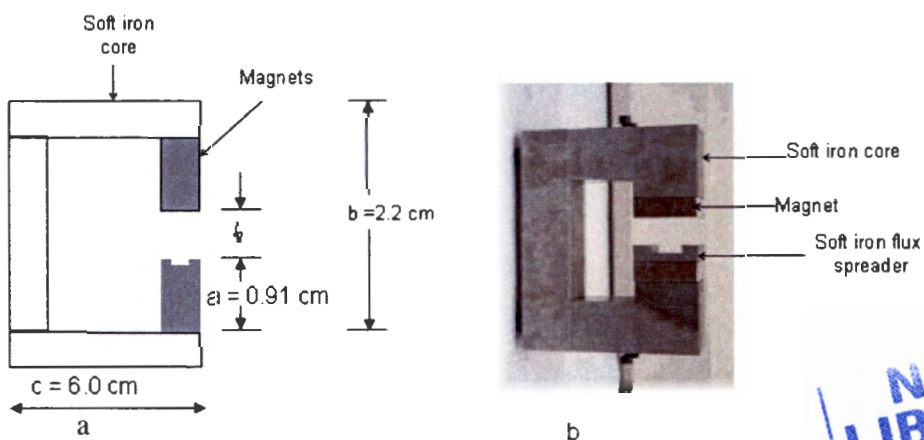

Figure 18. The configuration of the magnetic circuit

Figure 18 (a) is the schematic diagram of the configuration of the magnetic circuit, (b) is a picture of the magnetic circuit used. It is required that the magnets must produce magnetic field intensity, $B_g = 5000$ Gauss in the centre of the gap and the width required is 2.8 cm, this value was chosen for the design to ensure that the entire width of the flight will be in the region of the magnetic field. Therefore from Equation 4.3 the cross-sectional area for the magnet can be calculated

Given l_g = 7.5 cm

B_d = 12 000 (Refer to Figure 29)

δ_g = 21 cm^2

Therefore $\delta_g = \frac{5000\,\text{Gauss} \times 21\,cm^2 \times 6.7}{12\,000\,\text{Gauss}}$

= 58.625 cm^2

Therefore the cross-sectional area for each magnet piece will be 29.3 cm $\approx$ 30 cm. The two magnet pieces are held together by a soft-iron-core to make a c-shaped magnetic circuit. The magnets have specially been shaped by attaching a soft iron flux spreader so that a non-uniform magnetic field is produced for the deflection of Ag-atoms.

4.1.4 Vacuum system

The experiment was performed at a vacuum pressure of 1x 10^{-5} Torr, because the vaporization temperature is reduced to $\pm$ 600 °C at this pressure and also to reduce the collisions between the atoms. The system consists of two pumps, the rotary vane pump which pumps to 1 x 10^{-2} Torr and the turbo-molecular pump which pumps from 1 x 10^{-2} to 1x 10^{-5} Torr. The vacuum was monitored by two gauges, the Pirani gauge for low vacuum measurement and the Penning gauge for high vacuum measurement. The vacuum pressure of the system was maintained by keeping the rotary vane pump and the turbo-molecular pump on at all times during experimentation.

5. Results

5.1. Theoretical results

5.1.1. Effect of the magnetic field intensity (B) on deflection (z) of Ag-atoms

In order to determine the effect of the magnetic field intensity on deflection (z) of Ag-atoms, Equation 3.7 (which has been repeated here for convenience) was used to calculate the deflecting force acting on the Ag-atoms, a horizontal geometry was assumed in the calculations

$$F = \pm \mu_B \frac{\partial B_z}{\partial_z} \tag{5.1}$$

where F = deflecting force

μ_B = magnetic moment of Ag-atoms

$\frac{\partial B_Z}{\partial z}$ = field gradient

From the Equation 5.1 it can be seen that the force acting on Ag-atoms is directly proportional to the magnetic moment and to the gradient of the magnetic field. In the following calculations we have assumed that the force acting on the Ag-atoms is constant throughout the region of the non-uniform field and therefore the Ag-atoms will move with a constant acceleration. In the calculation it has been assumed that the F_y and F_x are negligible and as a result F_z represents the maximum force experienced by Ag-atoms. Using Equation 3.7 we calculated the deflecting force acting on the Ag-atoms for different values of the magnetic field gradient, $(\partial B_z / \partial z)$,

For $\frac{\partial B_Z}{\partial z} = 6.25\ T/m$

$$F_z = \mu B_z \frac{\partial B_z}{\partial z}$$

$= 9.270154 \times 10^{-24}$ J.T^{-1} x 6.25 T/m

$= 5.80 \times 10^{-23}$ N

The rest of the calculations for the deflecting force under varying magnetic field gradient were calculated in the same way and the results are given in Table 1.

Table 1. The results obtained from the calculation of the deflecting force for varying magnetic field gradients.

Magnetic field intensity, B (T)	Magnetic field gradient $(\partial B_z/\partial z)$, (T/*m*)	Deflecting Force, F (N)
0	0	0
0.125	0.625	5.80×10^{-23}
0.250	12.5	1.16×10^{-22}
0.50	25	2.32×10^{-22}
1.0	50	4.64×10^{-22}
2.0	100	9.27×10^{-22}
4.00	200	1.85×10^{-21}

The results obtained for the Force were then used to calculate the distance of deflection, z for different values of the Force by using Equation 3.8 which has been repeated here for convenience.

$$z = \frac{1}{2}at^2 = \frac{1}{2}\frac{F_z}{m_{Ag}}\left(\frac{L_m}{v_{Ag}}\right)^2$$

where F = refer to Table1

m_{Ag} = 1.79×10^{-25} *kg*

L_m = 7.5 cm

v_{Ag} = 120 m/s (speed of Ag-atoms in the PBMR)

$$z\frac{1}{2}at^2 = \frac{1}{2}\frac{F_z}{m_{Ag}}\left(\frac{L_m}{v_{Ag}}\right)^2$$

$$= \frac{1}{2}\left(\frac{5.80\times10^{-22}\,\text{N}}{1.79\times10^{-25}\,\text{kg}}\right)\left(\frac{0.075\,\text{m}}{120\,\text{m/s}}\right)^2$$

$= 6.3 \times 10^{-5}$ m

= 0.063 mm

Table 2. The results of deflection of Ag-atoms for varying Force of deflection.

Force (N)	Deflection, z-(mm)
0	0
5.80×10^{-23}	0.063
1.16×10^{-22}	0.127
2.32×10^{-22}	0.253
4.64×10^{-22}	0.506
9.27×10^{-22}	1.011
1.85×10^{-21}	2.019

The obtained results for the deflection were then plotted versus the magnetic field intensity, the plot is given in Figure 19 below.

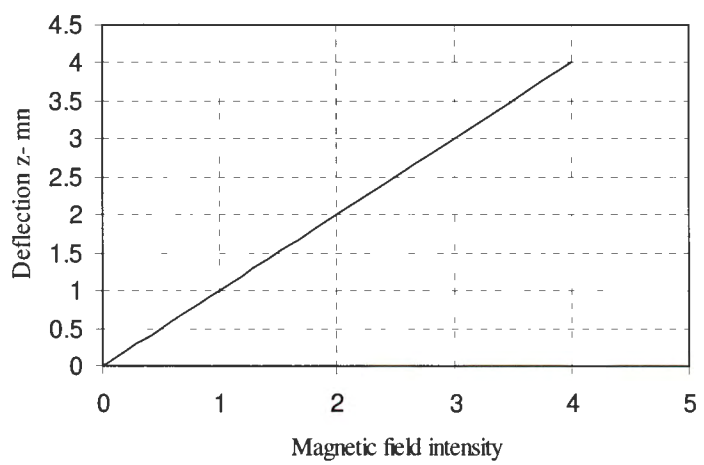

Figure 19. Graph of deflection versus varying magnetic field intensity.

The results obtained when plotted give a straight line graph and this shows that the deflection of Ag-atoms is directly proportional to the external magnetic field intensity and this is obvious from equation 5.1. An increase in the external magnetic field intensity results in an increased force and this leads to an increase in the deflection of Ag-atoms.

5.1.2 The effect of magnet length (L_m) on the deflection of Ag-atoms

In order to determine the effect of the length of the magnet (L_m)on deflection of Ag-atoms, Equation 3.8 was used to calculate the deflection of Ag-atoms for varying magnet lengths (L_m) for the same field gradient $(\partial B_z/\partial z)$ =25T/m and the results obtained are given in Table 3.

Table 3. Results obtained for the calculation of deflection (z) for different magnet lengths and same field gradient (25 T/m)

Magnet length L_m (*mm*)	Deflection, z (*mm*)
0	0
100	0.445
200	1.78
300	4.00
400	7.12
500	11.2

The results obtained for the deflection were then plotted versus different magnet lengths and the graph is presented in Figure 20.

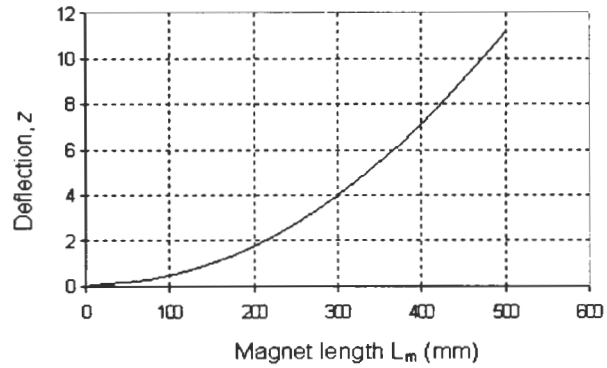

Figure 20. Graph of deflection versus different magnet lengths.

The results demonstrate that the increase in the deflection of Ag-atoms is quadratic as it was expected form the equation 3.8. This is due to the fact that the longer magnet results in an increased time in the magnetic field and therefore the Ag-atoms will be greatly deflected.

5.1.3 The effect of velocity (v) on deflection (z) of Ag-atoms

In order to determine the effect of velocity on the deflection of Ag-atoms, Equation (3.8) was used to calculate deflection (z) of Ag-atoms for different values of velocity (v) under different magnet lengths (L_m). Results are given in Table 4.

Table 4.Results for the calculation of deflection for different magnet lengths and different velocities.

velocity, (v) (m/s)	Deflection z (m) $L_m = 0.3$ m	Deflection z (m) $L_m = 0.6$ m	Deflection z (m) $L_m = 0.9$ m
15	2.56×10^{-1}	1	2.31
30	6.4×10^{-2}	2.56×10^{-1}	5.76×10^{-1}
45	1.6×10^{-2}	6.4×10^{-2}	1.44×10^{-1}
60	4.0×10^{-3}	1.6×10^{-2}	3.6×10^{-2}
120	1.0×10^{-4}	4.0×10^{-3}	9.0×10^{-3}
240	2.5×10^{-4}	1.0×10^{-4}	2.5×10^{-3}

The results for deflection versus velocity for different magnet lengths are plotted in the results are given in Figure 21.

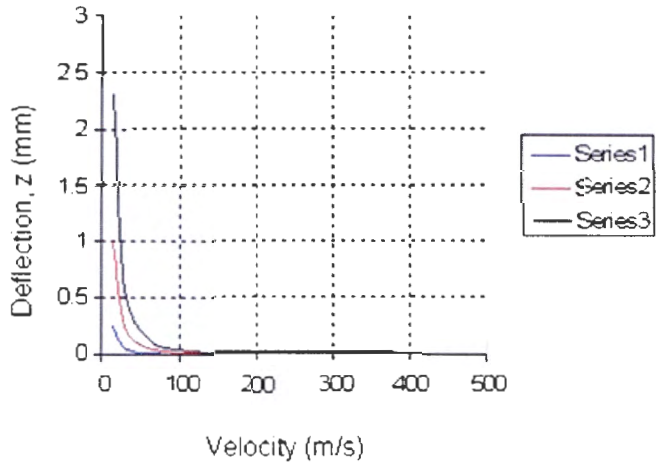

Figure 21.Graphs of deflection versus velocity for different magnet lengths and different velocities.

The results obtained from the graph show that the deflection of Ag-atoms varies as the inverse square of the velocity for a fixed magnet length L_m. Therefore at high velocities it is important to use longer magnet lengths so as to increase the deflection of Ag-atoms.

5.2 Experimental results

This section discusses the experimental procedures and the experimental results obtained., and is discussed as follows:

i. Establish the limits for the detection of silver in the model under vacuum.

ii. Shooting of a collimated beam of Ag-atoms to the target plate under vacuum.

iii. Deflection of Ag-atoms using magnets.

5.2.1 Establishing of detection limits

The limits for the detection of Ag were first established starting with the target plate placed 12.5 mm away from the oven exit and the experimental procedure taken is as follows;

- The equipment was thoroughly cleaned and wiped with ethanol to prevent the contamination of silver.
- All connections were then put together.
- The vacuum was first drawn with a rotary pump until a vacuum pressure of 2.6 x 10^{-2} mbar was obtained.
- Thereafter, the turbo-pump was started and vacuum was drawn until a vacuum pressure of 1 x 10^{-5} Torr was reached.
- The DC power supply was connected to the model through the terminals and the Ag-evaporation was started initially with 10 Watt and increased by a factor of two every 15 min until 350 Watt was reached. At this stage the temperature reading was ± 600 °C. Then, the vaporization was carried on until visible traces of Ag could be observed on the target plate.
- Thereafter, the path length of Ag-atoms was increased by lifting the target holder up to a specified position and the experimental procedure was repeated until a point was reached where Ag could not be observed on the target plate.

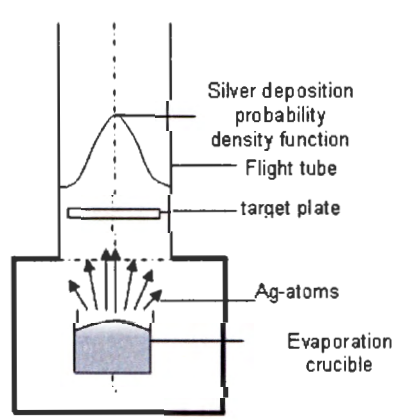

Figure 22.Schematic layout of the oven and flight tube.

Figure 22 shows the schematic layout of the oven and the flight tube. In the sketch, an Ag-pellet is vaporized in the oven and the beam exits vertically into the flight tube thereby hitting the target which is placed 12.5 mm away from the oven exit. A vertical position was chosen so that there is more chance of getting a maximum number of silver atoms through the collimator as opposed to the horizontal position; where gravity could bias the deflection.

5.2.1.1 Results for establishing of limits

Figure 23 shows the results obtained for the establishment of limits for the detection of silver. The target was placed at different positions from the oven exit as indicated on each picture and each time the depositions were observed. It is therefore concluded from these results that in the MSM the deflection of silver could be carried out for up to 75 mm.

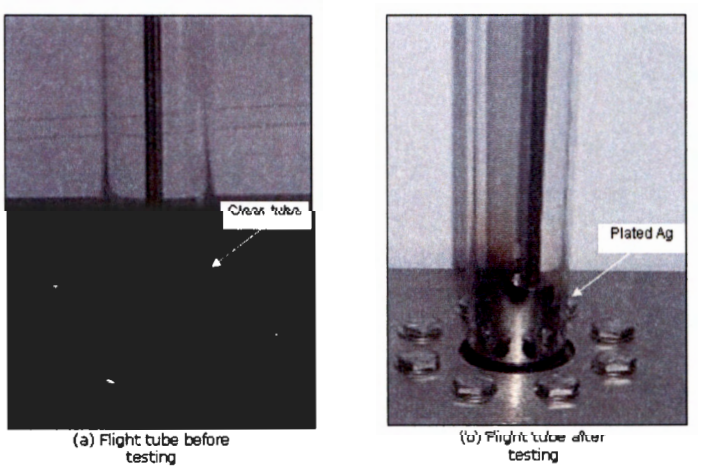

Figure 23. The picture of the flight tube (a) before the test (b) after the test.

The picture for each of the target plate for each of the different target distances from the collimator for different measurements is shown in Figure 24.

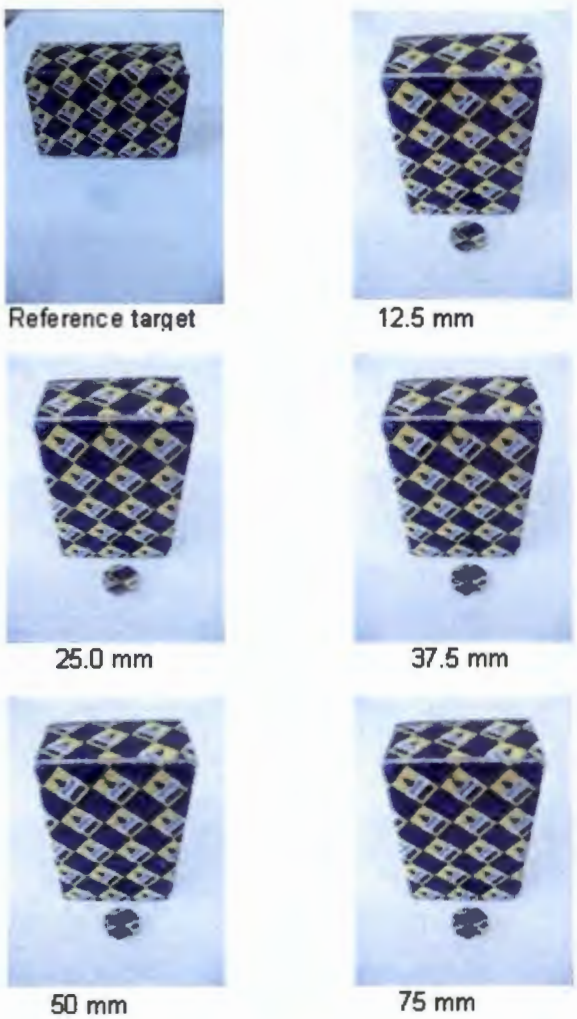

Figure 24. The results obtained for the establishing of limits, the pictures are for different target distances and at each distance an Ag-deposition was observed which formed a mirror on the target.

Figure 24 shows the appearance of the target during the establishment of limits for the detection of Ag within the flight tube. The target was placed at different positions from the oven exit as indicated on each picture and each time a perfect mirror was formed on the targets. This was as a result of the deposition of Ag-atoms on the target. It was therefore concluded from these results that in the MSM the deflection of Ag could be carried out for up to 75 mm.

5.2.2. Deflection of Ag-atoms

In order to carry out the deflection of Ag-atoms the beam was first collimated by inserting a nozzle with a 2 mm aperture inside the flight tube so that a confined spot on the target can be obtained that can be used as a reference. The experiment was first carried out at 12.5 mm without magnets and the procedure followed is the same as that for the establishing of limits. After a reference spot was obtained on the target, the magnets were placed around the flight tube and the experiment was repeated for the same target length.

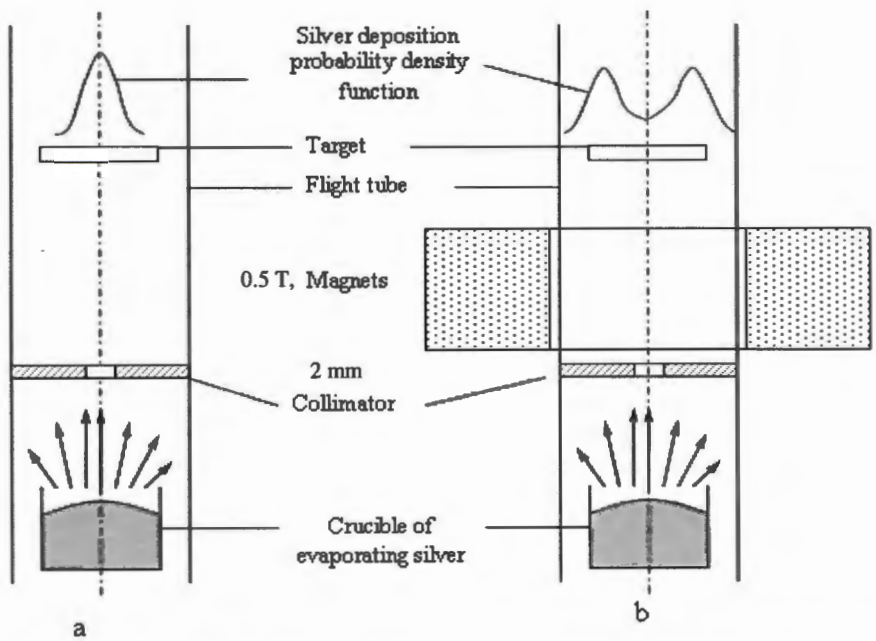

Figure 25. Schematic layout of the experimental set-up for the deflection of Ag-atoms.

Figure 25 (a) is the schematic layout of the experiment without the magnets; (b) is the schematic layout of the experiment with the magnets around the flight tube. The expected results is that when the magnets are placed around the flight tube the beam should split into two parts depending on the orientation of the spin magnetic moment. In this set-up the Ag-atom beam travels about 10 mm after exiting the magnetic field before reaching the target (refer to Figure 14 and Section 3.8). This will result in an increase in the angle of deflection and therefore the deflection will be more.

5.2.2.1. Results for the deflection of Ag-atoms

The picture of the experimental results is shown in Figures 26 and 27.

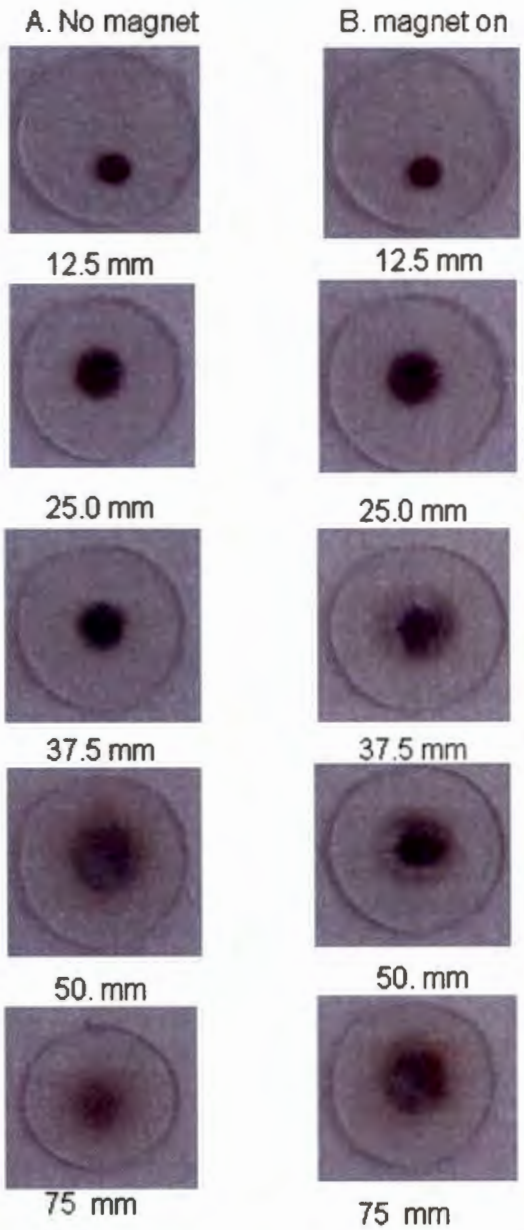

Figure 26. Results obtained for the deflection of Ag-atoms.

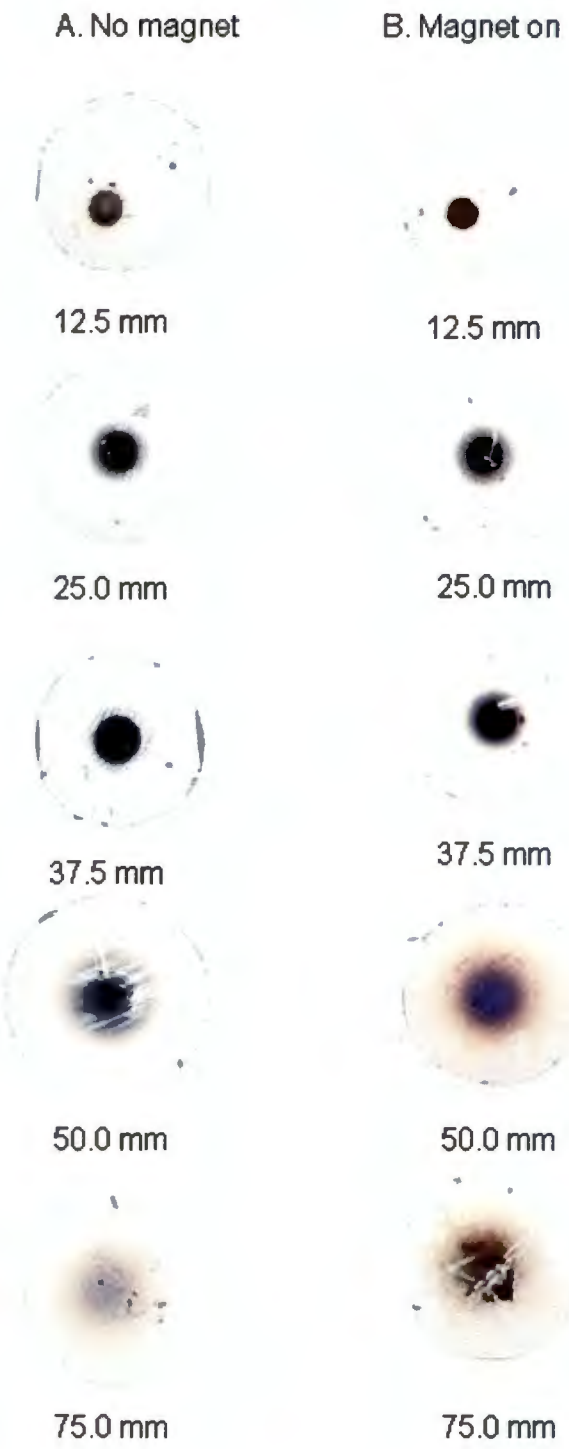

Figure 27. Results obtained for the deflection (Picture taken with light shined through the samples).

Both Figures 26 and 27 show the pictures of the samples taken with a normal camera and with a light shined through them respectively. The samples underneath A are for different target distances, 12.5 mm, 25.0 mm, 37.5 mm, 50.0 mm and 75 mm and this is with respect to the oven exit without the magnets. The sample underneath B are for the same target distances as stated above but with magnets of varying lengths placed around the flight tube with respect to the target position.

From both Figure 26 and 27 at 12.5, 25.0, 50.0, and 75 mm it is somewhat difficult to visually identify the differences between the silver deposition without and with magnets. At 12.5 and 25.0 mm the target was at its lower position and from the (theoretical calculations using equation 3.8) the deflection is inversely proportional to the magnet length (L_m) and this is in agreement with the theoretical results. However when the target is placed further up, at 37.5 mm there is a clear difference between the diameters of the spot of Ag deposited on the target as shown in Figure 28.

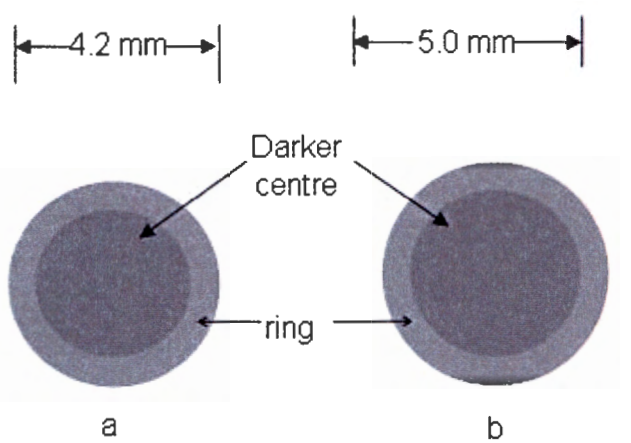

Figure 28.The schematic diagram of the appearance of the sample at 37.5 mm.

In Figure 28, a refers to the target without magnets, and b refers to the target with magnets placed around the flight tube. The visual inspection of this sample shows that;

1. There is a difference of 19 % between the diameter of the silver deposited without and with magnets and this is shown schematically in Figure 28 above.

2. There is a definite ``ring'' visible when we tilt the samples to get the good reflection of the light and this is also bigger with the magnets.
3. Depending on exactly how we tilt the target centre area the deposited silver appear to be either shiny or less; nothing in between; no different shades of color.

6. Discussions and conclusions

The theoretical calculations performed for the design of the magnetic scrubber model reveal that the deflection of Ag-atoms is entirely dependent on the following;

1. Magnetic field intensity - An increase in the intensity of the magnetic field gradient leads to an increase in the force and this ultimately results in greater deflections.
2. Velocity of atoms - The higher the velocity the shorter the time spent in the region of the magnetic field and the less the atoms will be deflected. Conversely, the lower the velocity the more time will be spent in the field region and the more they will be deflected.
3. The path length - Long path lengths result in more time spent in the field region and the greater the deflection.
4. Gap length - The gap length of a magnetic circuit is an important factor that should be considered in the design process because it is inversely proportional to the magnetic flux density in the centre of the gap. This means that bigger gap lengths will results in less magnetic flux density in the centre of the gap and this leads to less deflection of the Ag-atoms.

In the experimental process many unforeseen problems had to be overcome and the following were the main problems encountered which had to be addressed;

i. The machineable ceramic used to make the crucible could not take more than five firings, it had to be checked and changed often.

ii. The heating element used was also vaporizing at a vacuum pressure of 10^{-5} Torr and therefore needed to be changed after about three runs.

iii. The thermocouple needed to be correctly inserted at the mouth of the crucible otherwise an inaccurate temperature reading will be obtained.

The predicted results (refer to Figure 25) for this experiment was that the beam will split into two parts. It was therefore expected that there will be two dots in the target plate distributed above and below the point where there was no magnetic. But in the experimental result we have only a change in ring diameter when we go from magnetic field intensity on-to-off (refer to Figure 28). At this point the expected deflection of Ag-atoms at 600 °C, velocity = 366 m/s (probable speed of Ag-atoms from the oven) and the field gradient $\partial B_z/\partial z = 18\ T/m$ in the experiment

$$z = \frac{1}{2}at^2 = \frac{1}{2}\frac{F}{m_{Ag}}\left(\frac{L_m}{v}\right)^2$$

where

$$F_z = \mu_B \frac{\partial B_z}{\partial z} = 9.270154 \times 10^{-24}\ \text{J.T}^{-1} \times 18\ \text{T/m} = 1.66 \times 10^{-22}\ \text{N}$$

m_{Ag} $= 1.79\times10^{-25}\,\text{kg}$

L_m $= 37.5\ \text{mm} = 0.0375\ \text{m}$ (refer to Figure 25)

v $= 366\ \text{m/s}$, probable velocity of atoms from the oven

$$= \frac{1}{2}\frac{1.66\times10^{-22}\,\text{N}}{1.79\times10^{-25}\,\text{kg}}\left(\frac{0.0375\,\text{m}}{366\,\text{m/s}}\right)^2$$

$$= 4.9 \times 10^{-6}\,\text{m} = 4.9 \times 10^{-3}\,\text{mm}$$

This distance of deflection is very small to effect the total splitting of the Ag-atom beam instead a concentric ring was observed to have been formed with different shades of colour. This could be attributed to the higher probable velocity (366 m/s) at which Ag-atoms were traveling at when coming out of the oven (refer to Figure 21)

Based on this observations it is noted from the experimental results that shorter magnet lengths and shorter target positions with respect to the oven exit, results in atoms experiencing less or no deflection. Hence by increasing the distance of the target and

using longer magnet lengths there is a slight increase in the deflection of the atoms. It is therefore concluded that it is important to deflect the atoms over a long distance as this allows them to experience the deflecting force for a long time and greater deflections can be achieved.

In the actual PBMR the silver atoms move along with helium at a temperature of about 950 °C and pressure of 9 MPa. It is not feasible in our experiment to evaporate silver at these conditions since the boiling point of silver is affected by pressure, e.g. at a pressure of 3 bar the boiling point of silver is already high at 2700 °C. Also, that the probable velocity of the Ag-atoms at the 950 °C will be 453 m/s and the deflection will even be lesser. However at low vacuum it is easy to boil silver, at a vacuum pressure of 10^{-5} Torr the boiling point of silver is only ± 600 °C. It was therefore decided to establish the possibility of deflecting silver under vacuum conditions.

Even under vacuum it is unlikely that the magnets will deflect silver from the centre of the hot-pipe to the wall. For instance at a distance of 37.5 mm (as observed in Figure 28) the diameter of the silver deposit grew from 4.2 mm to 5 mm, in order to grow to a diameter of 2 m would by simple proportion be:

$$x\,(\text{mm}) = \frac{37.5 \text{ x } 2000}{5 - 4.2} = 93\,750 \text{ mm} \approx 94 \text{ m}$$

The available length of the hot-pipe in the present PBMR design is only about 6 m. Further studies on this technique reveal that at high pressure even longer distances than the calculated 94 m will be required for deflecting silver atoms (Cronje P.M., 2006).

6.1. Recommendations

The current technology does not provide for the required magnetic field intensity in the centre of the large pipe diameter that can deflect Ag-atoms to the pipe wall. Also the operating temperature limit of highest strength permanent magnets that are commercially available (N50 and N45SH) is only 150°C. This is in opposition to PBMR which is operating at a minimum operating temperature of 950 °C as these magnets will lose their strength when exposed to such temperature. Therefore methods for effectively removing silver from helium must be devised; this could include using electric force fields, laser ionization and centrifugal force techniques.

7. Bibliography

http://hyperphysics,phy-astr.gsu.edu/hbase/spin.html.

http://hypertextbook.com/fact/2000/ annalendoc.shtml

http: if .ufrgs .br /~betz / quantum /SGPeng .html.

http://www.fas.org/sgp/othergov/doe/lanl/lib-www/la-pubs/00326397.pdf

http:www.pbmr.co.za.

http://msc.phys.rug .nl/quantummechanicss/stern.html.

http:www. Plato .Stanford .edu/entries/ physics-experiment/app5.html.

http://wwwupscale.utoronto.ca/generalinterest/harrisso/sterngerlach.html.

http://en.wilkipedia.org/wiki/gamma ray.

(http://www.overunity.com.com/index.php?topic),

Atkins, P.W., (1998), Physical chemistry, 6th Edition. Oxford University press.

Cronje, P.M., (2007), Verification of PBMR-MIS (Report), iThemba LABS, Faure.

Duderstadt, J.J.,Hamilton L.J., (1976), Nuclear reactor analysis, Canada, John Wiley & sons .

Funk, E.G., and Wiedenbeck, M.L.,(November 1958), Decay of Ag-110m, Physical review, Vol. 112 (No 4), p 1247-1251.

George, A.P., (August 2001), Introduction to Pebble Bed Modular Reactor; (PBMR) Document no: 009949-1851.

Gauntreau, R., Savin, W. Modern physics, 2nd Edition, Schaums's outlines, McGraw-Hill.

Gregg, King, C.D., Nuclear power systems, 2nd Edition. Macmillan.

Heather, J., MacLean, Ronald G.Ballinger, (2004), Silver ion implantation and annealing in CVD Silicon Carbide: The effect of temperature on silver migration, Paper no: 23, 2nd international topical meeting on High Temperature Reactor Technology, Beijing, China, September 22-24.

Inamati, S. et al., Gaseous and metallic fission products transport characteristics of a modular pebble HTGR during loss of cooling accident, DOE Contract no.DE-AT03-84 SF 11963-GA Project 7800.

Kousaku, F., et al. (January 1985), Migration behavior of fission products in and from the spherical High-temperature Reactor fuel elements, Vol. 69 p 368-369.

Krane, K.S., 1987, Introductory Nuclear Physics, United States of America, John Wiley and Sons.

Kuczynski, L., (June 2004), Magnetic Isotope Scrubber presentation.

Leena Joseph et al., (2007) Standardization of silver 110m at BARC, India, Journal of Metrology society India, Vol. 22 (No 4) p 225 -229.

Liebermann, J., (June 1998), The Stern-Gerlach experiment, Department of physics, Massachusetts Institute of Technology Cambridge No 02139.

Martzer, D., (2004), PBMR project status and the way ahead" Paper No: A04 .2nd International Topical Meeting on High Temperature Reactor Technology, Beijing China , September 22-24.

Marvin, B. S., (2007) Nuclear power for clean, safe and secure energy independence, DOI 10.1108/14636680710837307. Vol. 9 (No 6), p 47-60.

van der Merwe, J.J., (2004), Development and validation of fission product release models and software at PBMR, Paper No: C : 18. 2nd International topical meeting on high temperature technology, Beijing China, September 22-24.

Nabielik, H., et al. Core heat-up and accidental simulation with HTR fuel elements, Kernforschungsanlage Julich GmbH.

Ogawa, T., et al., (April 1985), Release of metal fission products from UO_2 kernel of coated particle, Journal of nuclear materials, Vol. 135, p 18-31.

Petti, et al., (June 2003), Key differences in the fabrication, irradiation and temperature accident testing of U.S and German triso-coated particle fuel and their implication on fuel performance, 1st International topical meeting on high temperature reactor technology, Nuclear Engineering and Design Vol. 222 (issue 2-3) p 281-297.

Phywe series of publications, systeme, Laboratory Experiments physics, PHYWE SYSTEME, GmbH.

Ponomarev-Stepnoi., et al. (2003), Development of fast helium reactors in Russia, Atomic energy, Vol. 94 (No.4) p 262-270.

Slabber, J., (2004), Pebble Bed fuel advantages, Paper No: B 15, 2nd International topical meeting on high temperature reactor, Beijing, September 22-24.

Stanley, R.C., Applied physical techniques, Fisika G 530-8-STA.

Stern-Gerlach Advanced Laboratory Physics, University of Wisconsin, Madison, Wisconsin 53706.

Syed, A., N., Electric machines and Electromechanics, 2nd Edition, Schaums's outlines. McGraw-Hill.

Taylor, H.W., Scott, S.A., (April 1959), Disintegration of Ag-110m, Physical Review, Vol. 114 (No 1) p 121-126.

Weinert, F., (1995), Wrong-Theory-Right Experiment : The significance of the Stern-Gerlach Experiments, Studies in the History and Philosophy of Modern Physics, Vol. 26 (No 1) p 75-86.

8. Appendices

8. A. Demagnetization curve for NIB magnets.

MMPA Material Properties for NdFeB

Material	$(BH)_{max}$ (MGOe)	B_r (Gauss)	H_c (Oersteds)	H_{cj} (Oersteds)
NdFeB 31/25	31	11200	11000	25000
NdFeB 35/19	35	12300	11900	19000
NdFeB 38/17	38	12500	12100	17000
NdFeB 40/14	40	12600	12300	14000
NdFeb 44/12	44	13500	11000	12000

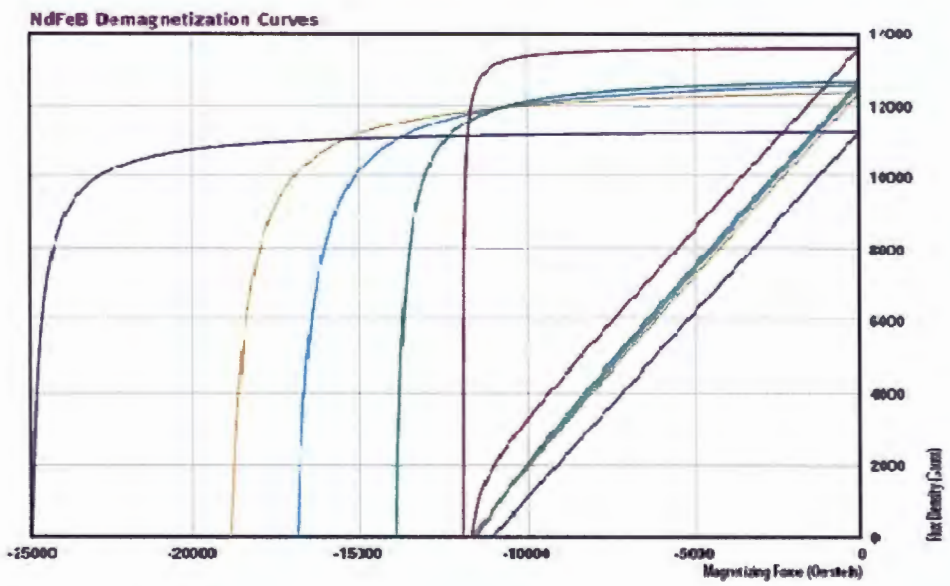

Figure 29. Demagnetization curve for NIB magnets.

8. B. A graph of vapour pressure of metals

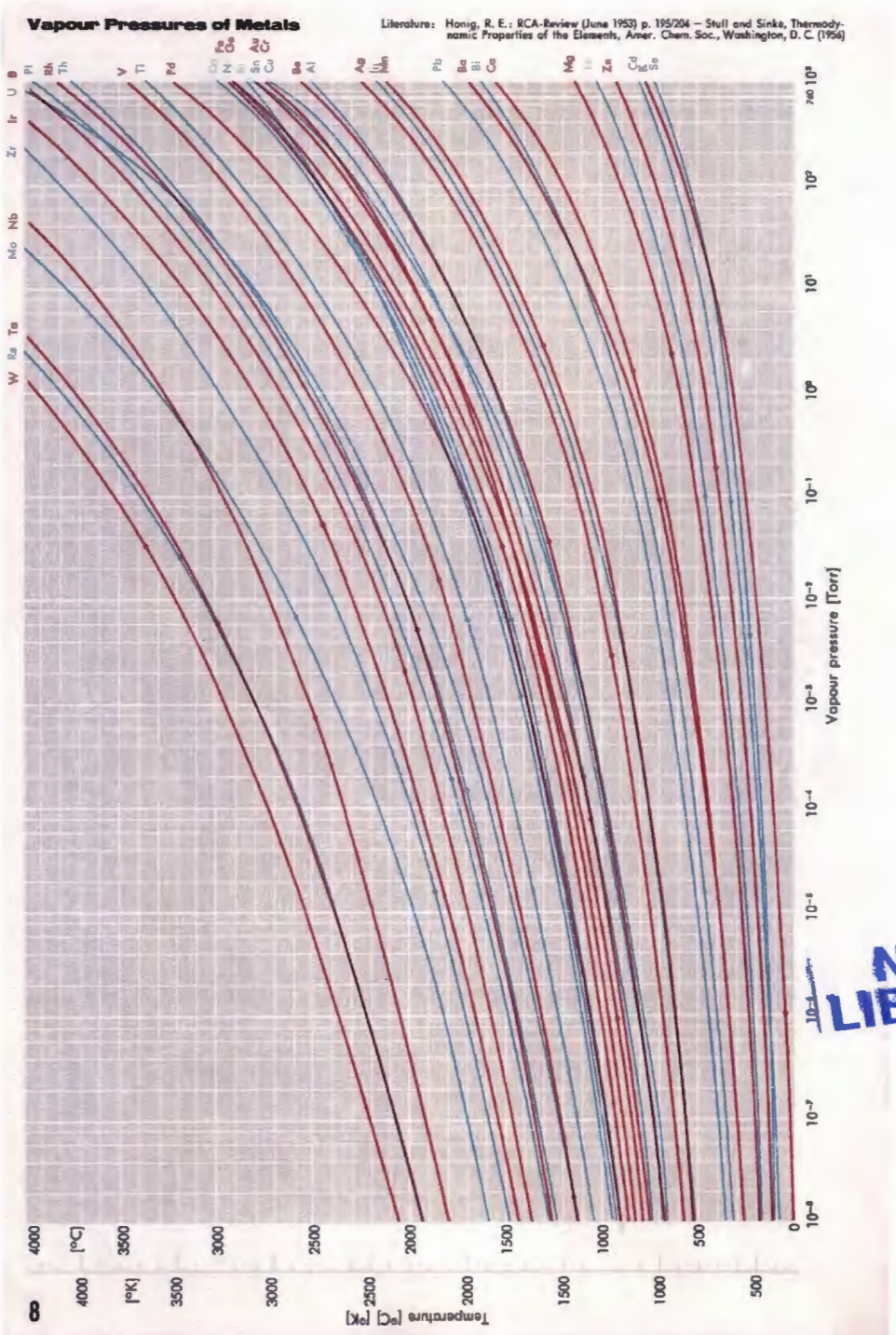

Figure 30. Graph of the vapour pressure of metals.

8. C. Manufacturing drawings

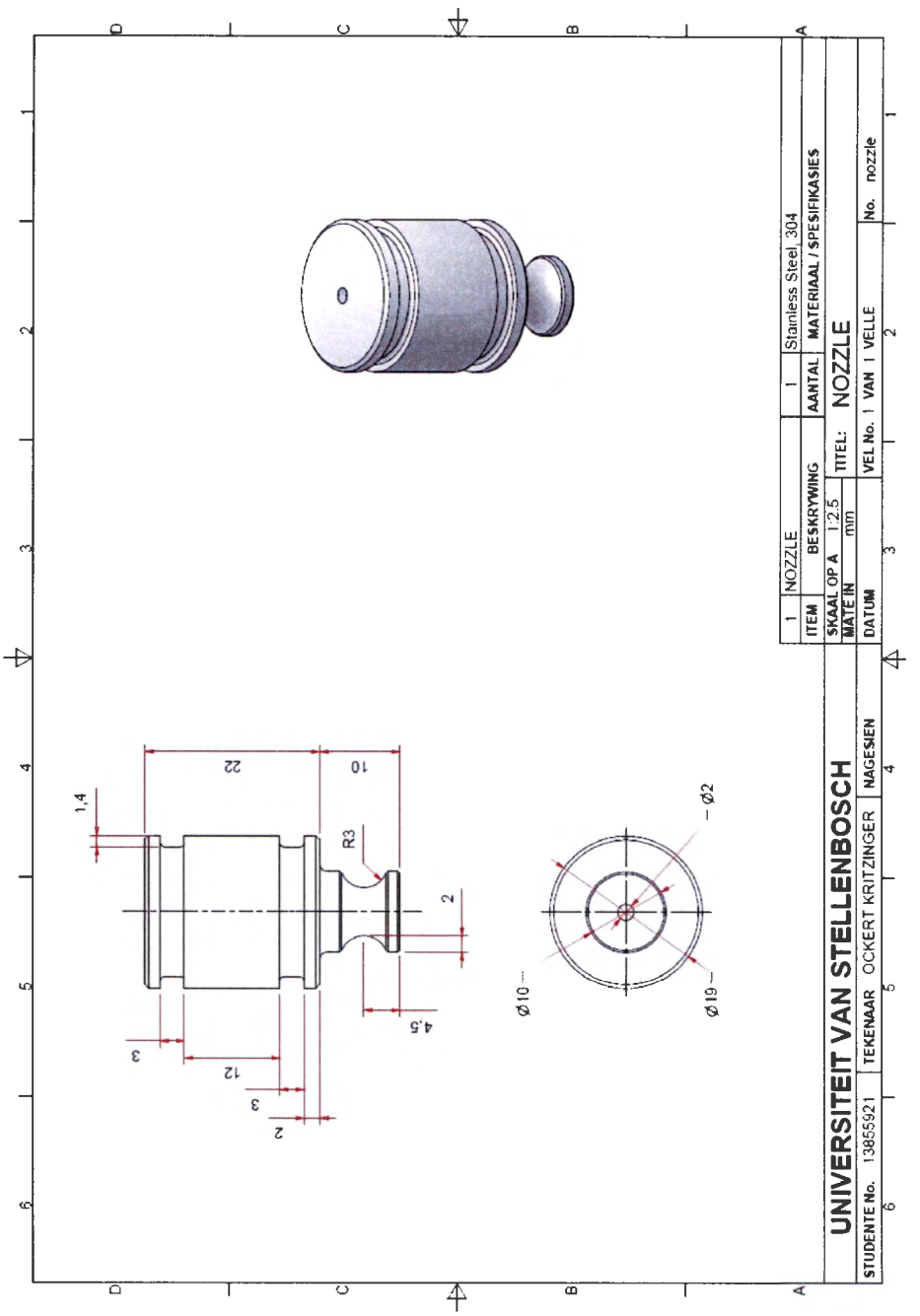

Figure 31. The nozzle.

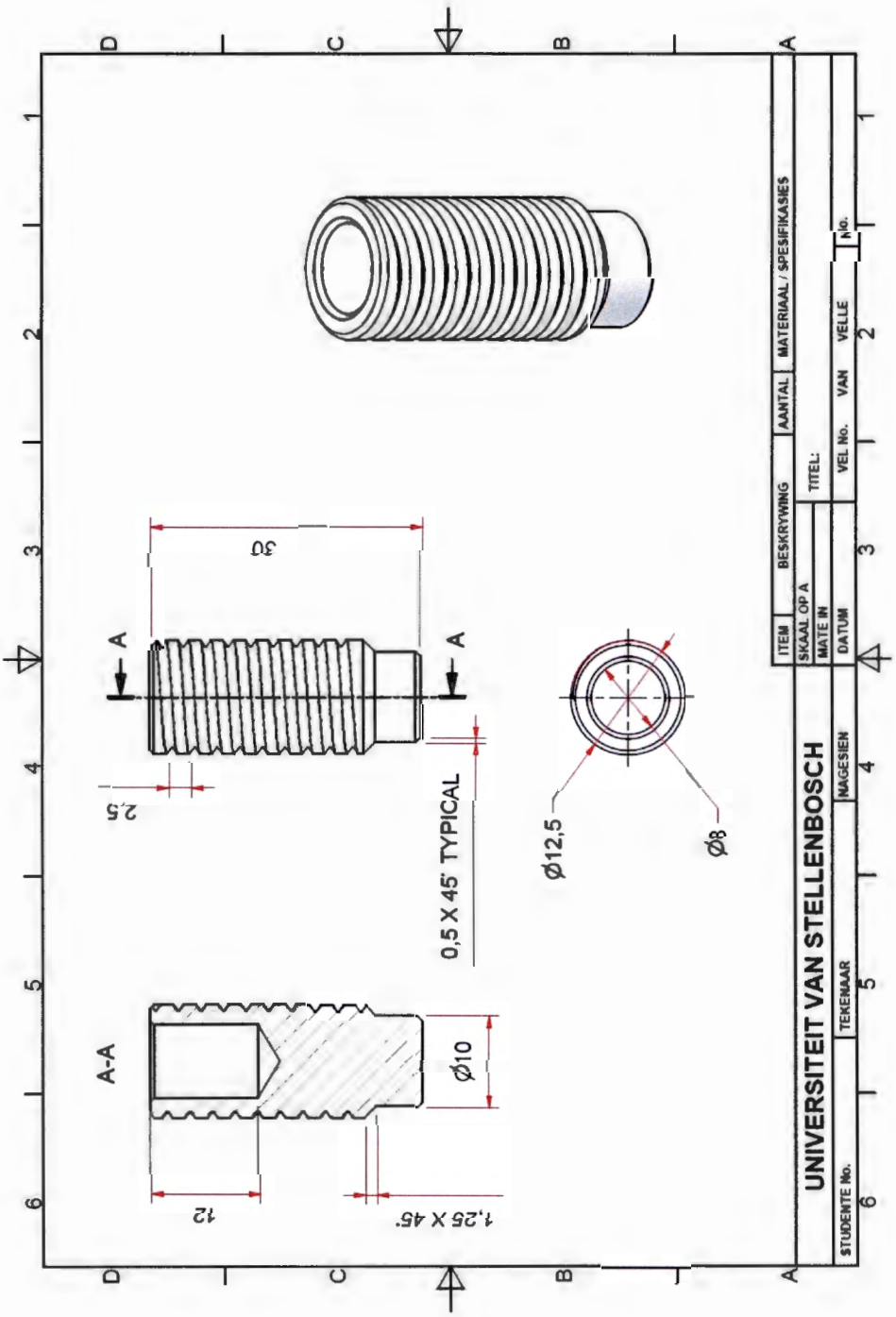

Figure 32. The crucible.

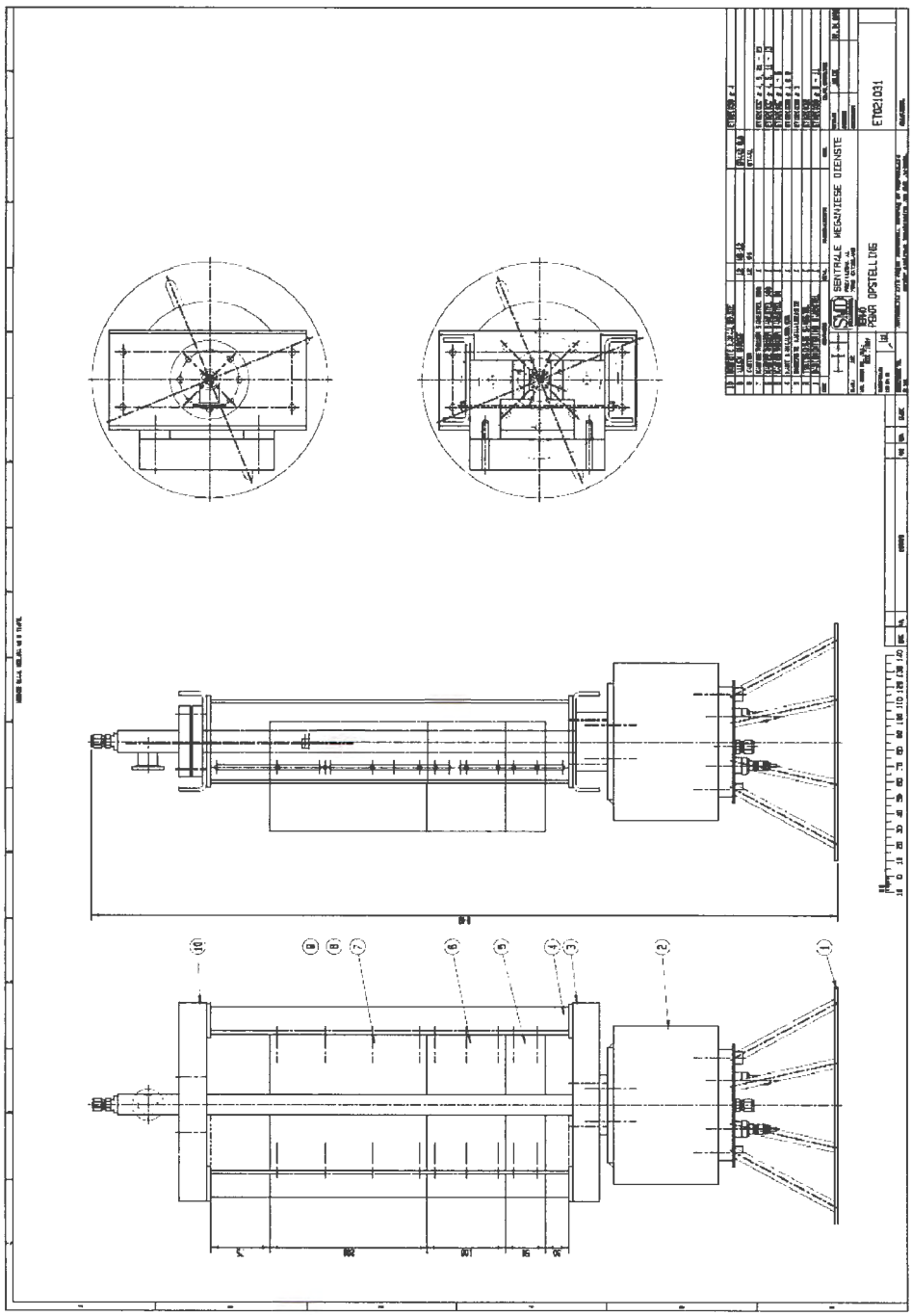

Figure 33. Drawing of the Magnetic Scrubber Model.

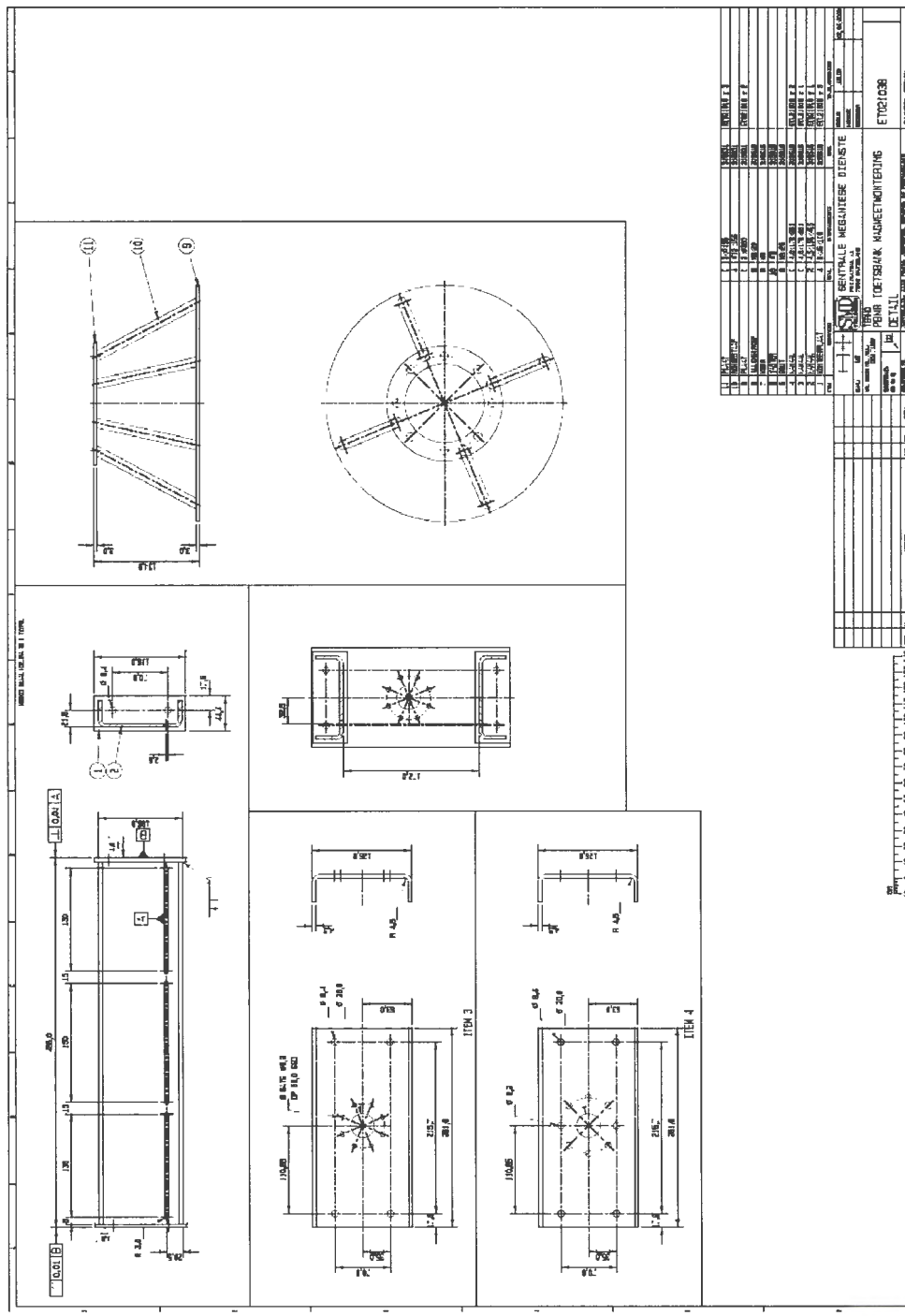

Figure 34. The support frame and the bottom flange.

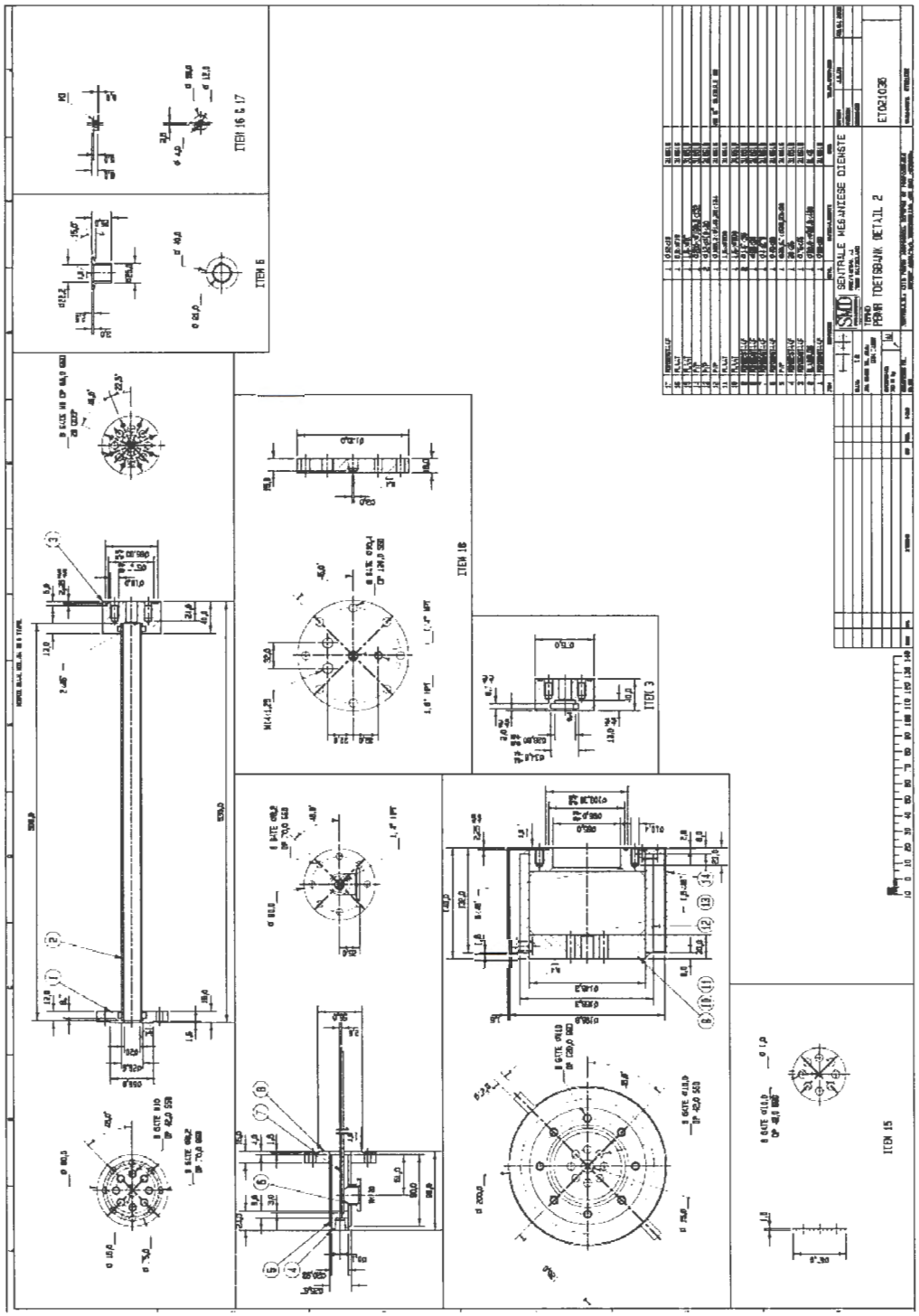

Figure 35. The flight tube and the oven components.

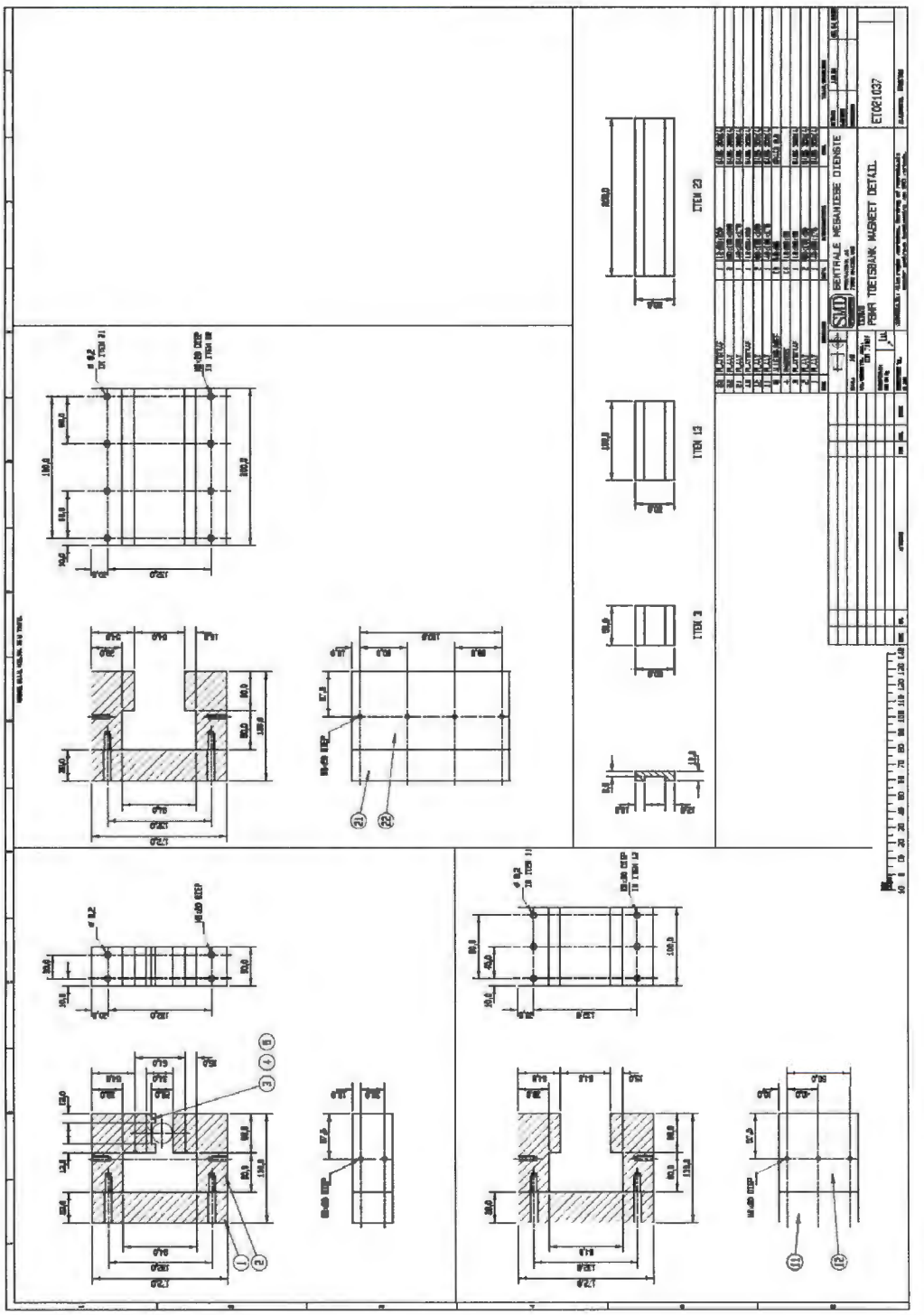

Figure 36. The magnetic circuit.

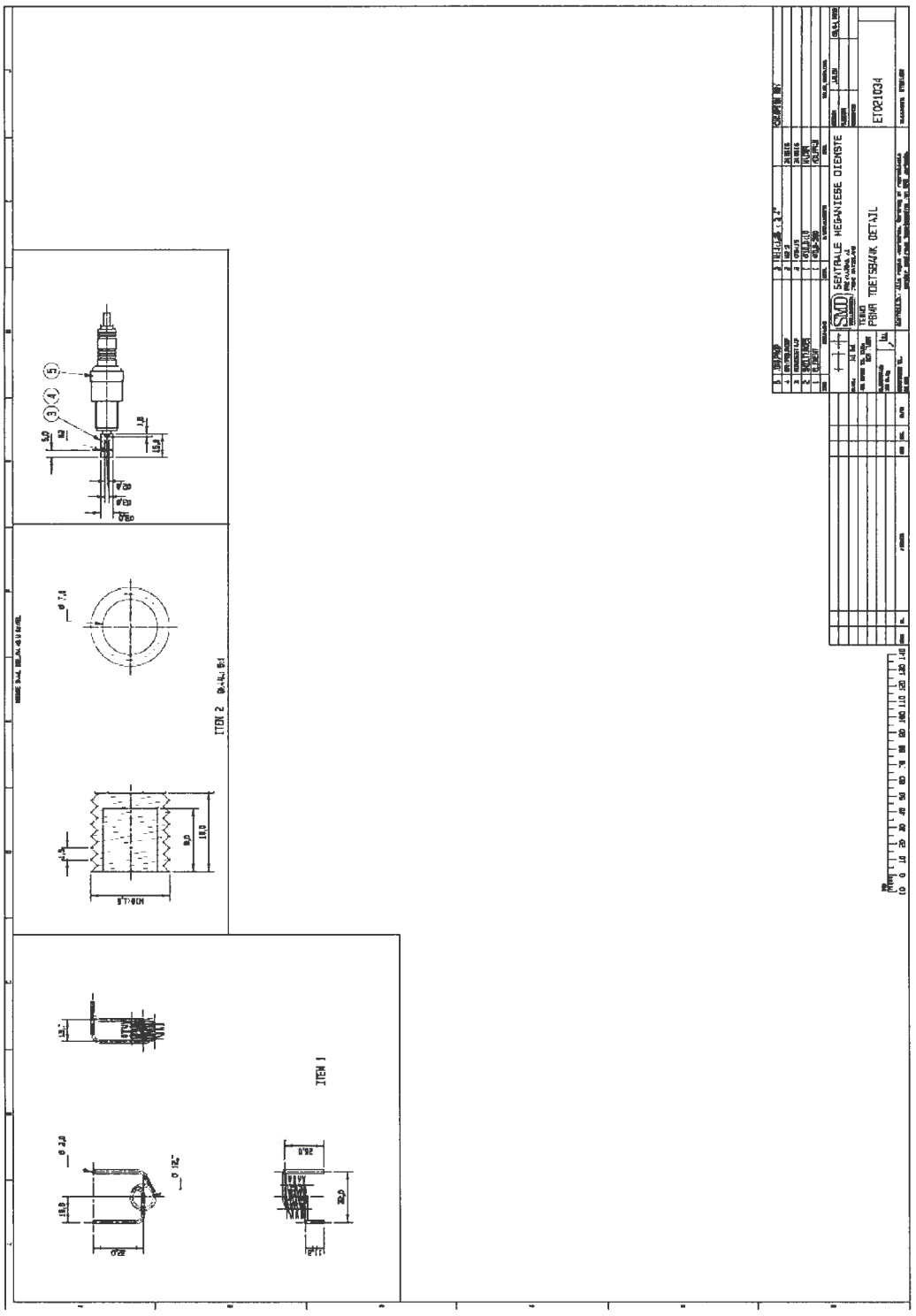

Figure 37. The crucible and the heating element.

D. Supplementary Data

D.1 General safety procedure and rules for the operation of the MSM

- 1. A good safety procedure must be adopted at all times during and after the operation of the MSM.

- The equipment must be thoroughly cleaned and be wiped with ethanol in order to prevent Ag contamination.

- All the screws must be tight.

- The glass tube must fit securely between the oven and the magnet frame.

- There must be adequate water supply for cooling the turbo-pump and ensure that the water is not blocked and there should be no leaks.

- Ensure that the insulation integrity of all the electrical leads is maintained.

- When drawing vacuum, always start the rotary pump first until about a vacuum pressure of about 1 x 10^{-2} Torr is attained and thereafter a turbo-molecular pump can be started and always ensure that the cooling water is on throughout operation.

- The laboratory is ventilated after the experiment.

2. Magnets

When working with magnets always:

- Put away the cell phone, credit cards and all the magnetic materials.

- Be careful with your fingers.
- Never put magnets on an unclean surface.
- Handle them with care, avoid dropping.
- Keep all electrical cables away from the magnets to avoid interference.

3. Temperature

The coolant water outlet must be kept below 56 °C.

4. Turbo-molecular pump

- Always ensure that the oil level is never below the minimum and it must be changed after several runs.
- Never jar or attempt to move the pump while it is still running.(the pump rotor can be destroyed)
- Never ventilate the vacuum chamber/manifold while the pump is still running.
- Never allow any dirt or metal filings to enter the pump.